Pergamon

Geochimica et Cosmochimica Acta, Vol. 67, No. 15, pp. 2857–2877, 2003

0016-7037/03 $30.00 + .00

doi:10.1016/S0016-7037(03)00086-3

U-Th-Pa-Ra study of the Kamchatka arc: New constraints on the genesis of arc lavas

ANTHONY DOSSETO,[1,*] BERNARD BOURDON,[1] JEAN-LOUIS JORON,[2] and BERNARD DUPRÉ[3]

[1]Laboratoire de Géochimie et Cosmochimie, IPGP-CNRS UMR 7579, 4 Place Jussieu, 75252 Paris cedex 05, France
[2]Laboratoire Pierre Süe, CE/Saclay, B.P. 2, 91190 Gif sur Yvette, France
[3]Laboratoire d'Etude des Méeanrsmes de Transfert en Géologie, CNRS-OMP UMR 5563, Université Paul Sabatier, 38 rue des 36 ponts, 31400 Toulouse, France

(*Received April* 15, 2002; *accepted in revised form January* 16, 2003)

Abstract—The ^{238}U-^{230}Th-^{226}Ra and ^{235}U-^{231}Pa disequilibria have been measured by mass spectrometry in historic lavas from the Kamchatka arc. The samples come from three closely located volcanoes in the Central Kamchatka Depression (CKD), the most active region of subducted-related volcanism in the world. The large excesses of ^{226}Ra over ^{230}Th found in the CKD lavas are believed to be linked to slab dehydration. Moreover, the samples show the uncommon feature of ($^{230}Th/^{238}U$) activity ratios both lower and higher than 1. The U-series disequilibria are characterized by binary trends between activity ratios, with ($^{231}Pa/^{235}U$) ratios all >1. It is shown that these correlations cannot be explained by a simple process involving a combination of slab dehydration and melting. We suggest that they are more likely to reflect mixing between two end-members: a high-magnesia basalt (HMB) end-member with a clear slab fluid signature and a high-alumina andesite (HAA) end-member reflecting the contribution of a slab-derived melt. The U-Th-Ra characteristics of the HMB end-member can be explained either by a two-step fluid addition with a time lag of 150 ka between each event or by continuous dehydration. The inferred composition for the dehydrating slab is a phengite-bearing eclogite. Equilibrium transport or dynamic melting can both account for ^{231}Pa excess over ^{235}U in HMB end-member. Nevertheless, dynamic melting is preferred as equilibrium transport melting requires unrealistically high upwelling velocities to preserve fluid-derived $^{226}Ra/^{230}Th$. A continuous flux melting model is also tested. In this model, ^{231}Pa-^{235}U is quickly dominated by fluid addition and, for realistic extents of melting, this process cannot account for ($^{231}Pa/^{235}U$) ratios as high as 1.6, as observed in the HMB end-member.

The involvement of a melt derived from the subducted oceanic crust is more likely for explaining the HAA end-member compositions than crustal assimilation. Melting of the oceanic crust is believed to occur in presence of residual phengite and rutile, resulting in no ^{226}Ra-^{230}Th disequilibrium and low ^{231}Pa excess over ^{235}U in the high-alumina andesites. Consequently, it appears that high-alumina andesites and high-magnesia basalts have distinct origins: the former being derived from melting of the subducted oceanic crust and the latter from hydrated mantle. It seems that there is no genetic link between these two magma types, in contrast with what was previously believed.

1. INTRODUCTION

Subduction zones are a unique tectonic setting where new continental crust is built and materials from the surface are buried in the deep Earth's interior. Studying this geodynamical setting is essential for better understanding the links between arc volcanism and slab fluxing, and to which extent the composition of the Earth's mantle is affected by recycling of surface materials. Indeed, one of the goals of studying subduction zones is to establish the mass balance between material transferred to the mantle wedge, and ultimately to the arc, and the material recycled in the deep mantle.

Previous studies have shown that the mantle wedge is metasomatized by fluids produced during dehydration of the downgoing slab and by subducted sediments (e.g., Gill, 1981). Thus, arc lavas are thought to be a mixture of at least three components: mantle wedge, fluids extracted from the sinking slab and subducted sediments. As the sediment input to the Kamchatka arc is limited (Kepezhinskas et al., 1997), this location should allow to focus on the mechanisms of slab dehydration and its implications for arc magma genesis, in general.

U-series disequilibria are a powerful tool for studying geological processes for two reasons. Firstly, they provide time constraints on geological processes. Secondly, it can be assumed that the system is initially in secular equilibrium (equal activities for the nuclides in the decay chain). This enables to discriminate recent fractionation event as opposed to fractionation that preexisted in the mantle source. Most U-series studies of arc volcanism have focused on ^{230}Th-^{238}U disequilibria and shown that most arc lavas are characterized by ^{238}U excess. The most straightforward interpretation is that the source of arc lavas may have been enriched in U over Th several tens of thousands of years ago (e.g., Elliott et al., 1997; Hawkesworth et al., 1997; Turner and Hawkesworth, 1997; Turner et al., 1998). Few studies have also included precise ^{226}Ra-^{230}Th disequilibrium measurements (Chabaux et al., 1999; Turner et al., 2000, 2001). These studies have suggested that ^{226}Ra excesses over ^{230}Th, in arc lavas must result from fluid addition to the source. The time scale for this event is different from the timescale implied by ^{230}Th-^{238}U system. One interpretation is that there must have been a second stage of fluid addition to account for ^{226}Ra-^{230}Th data (Turner et al., 2000). Even fewer studies have looked at ^{231}Pa-^{235}U because of analytical difficulties in measuring protactinium abundances (Pickett and

* Author to whom correspondence should be addressed (dosseto@ipgp.jussieu.fr).

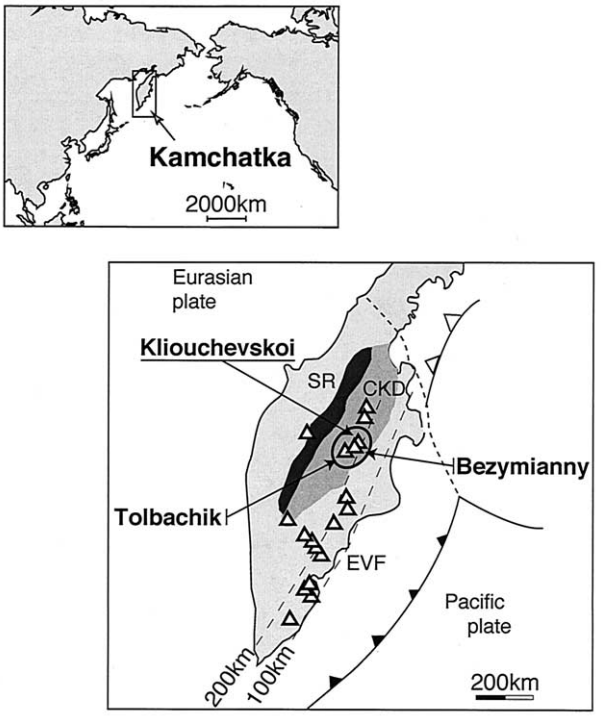

Fig. 1. Map of the Kamchatka peninsula. Triangles show the main active volcanoes. The studied volcanoes are located within the circle: Klyuchevskoy, Bezymianny and Tolbachik. SR, EVF and CKD are the three main volcanic provinces, namely, Sredinny Ridge, Eastern Volcanic Front and Central Kamchatka Depression, respectively.

Murrell, 1997; Bourdon et al., 1999b). As most arc lavas exhibit ^{231}Pa excesses over ^{235}U, it has been suggested that ^{231}Pa-^{235}U disequilibria essentially reflect a melting signature and that any previous fluid signature has been overprinted (Pickett and Murrell, 1997). Hence, ^{231}Pa-^{235}U disequilibria are potentially useful for understanding the mechanisms involved in melt production. In this study, we have attempted to integrate the information from these three radioactive systems. Since U and Ra are fluid-mobile elements compared to Th and Pa, the U-Th-Ra and U-Pa systems allow us to constrain the timing of slab dehydration and melting by combining the information they provide.

2. THE KAMCHATKA ARC

The Kamchatka Peninsula is located at the boundary between the Eurasian and Pacific plates (Fig. 1). This latter plate, which is 80 to 90 Ma old (Gorbatov et al., 1997), is being subducted at a rate of 8 cm/yr and a dip angle of 49° (DeMets et al., 1990). The Kamchatka arc is one of the most active arcs in the world. For instance, the production rate for Klyuchevskoy (the most productive arc volcano world-wide) has been estimated to 55×10^6 tons of magma/yr (Melekestsev et al., 1991). The 28 active volcanoes are divided into two groups: the Klyuchevskaya province located in the Central Kamchatka Depression (CKD), a large graben parallel to the trench, and the Eastern Volcanic Front (EVF) located to the south and trenchward. The Sredinny Ridge (SR) is the third main volcanic province but only one active volcano (Ichinsky) has been found in this region.

As shown previously (Hochstaedter et al., 1996), the composition of the lavas extends over both the tholeiitic and calc-alkaline fields defined by Miyashiro (1974). Various lithologies can be found, from high-MgO basalts to dacites and rhyolites. Trace element spidergrams normalized to N-MORB are typical of arc lavas with enrichment in Large Ion Lithophile Elements (LILE) and depletion in High Field Strength Elements (HFSE). Moreover, Nd and Pb isotope compositions plot within the Pacific MORB field. This observation has been previously used to infer that sediment contribution to magma composition must be low for the Kamchatka arc (Turner et al., 1998). In contrast, Sr isotope ratios are more radiogenic than in MORB, probably as a result of slab fluid addition (Turner et al., 1998). Turner et al. (1998, 2001) who have analyzed ^{238}U-^{230}Th-^{226}Ra in Kamchatka volcanics have suggested, for Central Kamchatka Depression, that a slab-derived fluid has been added to the mantle wedge ~150 ka before eruption of the lavas (Turner et al., 1998). Moreover, ^{226}Ra-excesses are believed to be fluid-derived rather than produced during melting (Turner et al., 2001).

The track of the Hawaii hotspot is being subducted in the northernmost part of the peninsula but there is no direct geochemical evidence for its involvement in the source of CKD magmas. Additionally, a recent study has shown that lavas from the northernmost volcano of the CKD (Sheveluch) show involvement of slab melts in their source (Yogodzinski et al., 2001).

3. GEOCHEMISTRY AND PETROLOGY OF THE SAMPLES

This study is limited to CKD volcanoes as they produce more magnesian and less silicic lavas than those from the EVF. To avoid across- or along-arc source variations, we focused on three closely related volcanoes forming the Klyuchevskaya group (Fig. 1); namely Klyuchevskoy, Bezymianny and Tolbachik (the sampling area is within a 50-km-diameter region). Major element, oxygen and hydrogen isotope data for 70 samples from these volcanoes, are reported in Pineau et al. (1999). Thirty-nine samples from this sample collection, have been analyzed for trace elements (Table 1) and 7, for long-lived radiogenic isotopes (Table 2).

Samples analyzed for U-series, are four basalts from Klyuchevskoy (KH78001, AXO-3/84, X117/83, K56P66), three from Tolbachik (PT33-1/82 from Plosky Tolbachik, T1475/1975 and PT30-4/1976 from the Great Tolbachik Fissural Eruption of 1975–1976), one basic andesite (M-1564-1) and two acid andesites from Bezymianny (B-8/4 and B-82). They all plot within the calc-alkaline field, except for one that is a high-K calc-alkaline rock (PT30-4/1976, see Fig. 2a). Most samples are high-alumina basalts or andesites whereas two are high-magnesia basalts (Fig. 2b). The texture of the samples is aphyric (T1475/1975, KH78001) to subaphyric with plagioclase and ferro-magnesian minerals (PT33-1/82, K56P66 and M-1564-1) or plagioclase and pyroxene minerals (X117/83). One sample (PT30-4/1976) shows a vesicular structure with glomerocrysts of plagioclase and olivine (<1 cm).

All the samples show typical trace element patterns of arc

Table 1. Trace element data for Central Kamchatka Depression lavas.

Sample	Zr	Hf	Ta	Ba	Sr	Cs	Rb	Sb	Cr	Co	Ni
Bezymianny											
Basic andesite											
40M84	100	2.41	0.157	358	363	0.6	21.9	0.17	120	27.4	26.7
15–58	102	2.54	0.158	383	361	0.76	22.6	0.19	113	27.2	8.5
81030	88	2.25	0.144	397	387	0.59	17.2	0.2	151	24.6	8
M-1564-1	97	2.69	0.169	407	323	0.89	25.3	0.19	119	27.8	28
Acid andesite											
B-8/4	140	2.96	0.198	519	323	0.73	26.1	0.28	90	19.7	19
B-8/5	101	2.52	0.158	387	353	0.77	21.6	0.28	68	20.1	12.8
B-85	109	2.65	0.161	388	369	0.76	20.8	0.28	69	20.5	13.9
B-77	100	2.75	0.161	402	347	0.76	22.2	0.28	23	20.2	14.9
B-82	108	2.82	0.17	431	353	0.81	24	0.31	18	20.4	12.1
M15-96	103	2.6	0.163	394	346	0.78	21.8	0.32	68	18.4	12
B-65	127	2.62	0.164	420	292	0.85	23.2	0.31	64	16.1	6.7
B-56	118	2.84	0.173	404	316	0.83	22.1	0.26	24	15.1	6
81024	164	3.96	0.288	439	413	0.61	23.2	0.22	36	3.7	4.3
Klyuchevskoy											
Basalt											
K77381	57	1.6	0.091	157	380	0.29	5.3	0.11		43.1	211
59-9	57	1.97	0.109	285	382	0.4	13.8	0.16	410	33.8	91
2-2	63	1.91	0.109	294	386	0.43	13.1	0.152	318	32.7	67
KH78001	75	2.02	0.119	322	350	0.45	14.9	0.18	263	34.4	69
KH78086	66	2.13	0.115	317	438	0.41	13.7	0.21	254	35.4	9.3
KH78017	70	2	0.11	281	229	0.43	12.8	0.18		34.1	71
KH78070	81	2.1	0.115	298	424	0.39	13.1	0.161	295	33.2	74
AXO-3/84	78	2.3	0.13	344	376	0.46	14	0.18	123	32.6	50
K77705	101	2.33	0.122	348	386	0.42	11.8	0.131	97	31.2	42
X117/83	100	2.58	0.144	393	417	0.49	5.5	0.198	67	28.5	29
K56P66	106	2.91	0.163	434	362	0.52	17.2	0.25	41	31.5	30.7
AXO-3085	100	2.72	0.153	415	367	0.51	16.7	0.25	55	29.0	28.7
AXO-40/87	104	2.79	0.159	412	385	0.51	16.6	0.221	45	30.3	25
K659-66	106	2.96	0.169	440	363	0.52	17.7	0.25	41	30.9	29.8
Basic andesite											
K77235	83	2.41	0.119	229	375	0.29	12.2	0.079	211	21.6	57
K77281	127	2.72	0.157	411	311	0.52	17.4	0.26	36	28.7	25
AXO-31	124	2.83	0.16	420	305	0.55	17	0.29	38	27.9	24
K585A	114	2.53	0.145	386	341	0.5	16.1	0.214	27	26.9	25
AB86-8	66	1.89	0.11	317	392	0.43	13.7	0.166	204	33.1	55
Acid andesite											
K657-68	275	6.79	0.405	622	361	1.91	53.2	0.69	23	14.4	8
K68604	298	7.73	0.473	710	309	2.2	60.8	0.738	17	15.8	10
K69-84	339	8.43	0.514	766	357	2.46	67.8	0.88	21	14.3	11
Plosky Tolbachik											
Basalt											
PT33-1/82	69	2.11	0.139	211	285	0.44	16.3	0.12	400	40	104
GTFE											
Basalt											
T1475/1975	204	5.6	0.44	480	461	1.7	54.2	0.37	119	32.5	60
PT30-4/1976	222	5.65	0.469	517	358	1.75	56.1	0.37	79	33.2	51
ST5-5/65/1976	129	3	0.22	344	385	0.67	22.82	0.12		28.2	20

Concentrations in ppm except for Au (ppb). GTFE: Great Tolbachik Fissural Eruption (1975–1976).

magmas with enrichment in Cs, Rb, Ba, U and Sr, and depletion in Ta (Fig. 2c). One sample (PT30-4/1976) exhibits much higher incompatible element concentrations and is characterized by a trace element pattern shifted upward compared with the other samples (Fig. 2c). It is possible that this sample is derived from a lower degree of melting. Samples are characterized by Pb and Nd isotope compositions within the range of MORB. The $^{87}Sr/^{86}Sr$ ratios (0.70334–0.70365) are higher than fresh MORB and could indicate an altered oceanic crust contribution. As there is no positive correlation between $\delta^{18}O$ and the water content and since water contents are low compared to altered MORB, Pineau et al. (1999) have concluded that our samples are devoid of alteration by local meteoric water.

4. ANALYTICAL PROCEDURES

Protactinium, Ra, Th and U concentrations were determined by Thermal Ionization Mass Spectrometry (TIMS) using isotope dilution techniques. The $^{230}Th/^{232}Th$ ratios were measured by TIMS at IPGP on four samples (M-1564-1, B-8/4, PT30-4/1976 and X177/83) and while the other samples were measured

Sc	La	Ce	Sm	Eu	Tb	Yb	W	As	Mo	Br	Ag	Au	Zn
26.4	7.28	18.6	3.02	1.13	0.508	1.93		0.68	0.4				
26.2	7.19	14.9	3.09	1.11	0.523	2.06		1	0.7	1.41			
24.9	6.99	13.2	2.62	1.03	0.447	1.78		1.14		0.83			
25.9	7.9	20	3.5	1.15	0.523	1.9	0.3	1.3	0.73	1.68	45	0.32	66
18.4	9.68	20.2	3.01	1.09	0.458	1.75		1.31	0.58				
19	8.09	19.5	2.76	1.03	0.451	1.85		1.97		1.76			
19	8.02	19.1	2.81	1.03	0.458	1.87		1.82	1.28	0.77			
19	7.9	19.2	3.13	1.04	0.479	1.8		2.1	0.86	1.22	70	1.4	66
17.8	8.3	20.2	3.17	1.04	0.478	1.8		2.48	0.91	0.8	87	1.4	65
17.5	8.06	19.5	2.8	1.03	0.445	1.77		2.25		2			
15.2	8.58	20.8	2.85	0.95	0.432	1.72		2.49		1.18			
14.1	8.33	21.1	2.98	1.05	0.44	2.02		0.75	0.98	1.7			
4.47	11.64	28.1	3.47	1.24	0.461	1.77		0.64	0.56				
33.3	4	9.5	2.4	0.82	0.42	1.7				0.6			
32.2	5.34	11.7	2.71	0.96	0.465	1.7							
32.6	5.82	12.3	2.69	0.89	0.454	1.56							
33.3	5.6	15	3.04	1.04	0.485	1.72	0.21	0.97	0.56	1.66	27	3.4	62
32	5.76	14.9	2.81	1	0.514	1.88		1.24	0.6	1.04			
33.8	15.18	33.3	4.8	1.12	0.74	2.8		0.75		1.8			
30.4	5.81	11.9	2.83	0.93	0.483	1.77							
29.6	6.6	16.8	3.3	1.07	0.56	2.2		1.2					
27.1	6.12	15.2	3.04	1.02	0.509	1.91							
25.6	6.45	13.9	3.4	1.24	0.579	2.04							
27.1	7.3	19	3.94	1.33	0.646	2.35		1.87	0.65	1.27	180	2.2	78
25.6	6.9	18	3.74	1.2	0.6	2.11		1.44	0.72	0.98	98	2.4	80
26.7	7.16	15.2	3.55	1.18	0.62	2.19							
27.7	7.7	19.2	4.01	1.34	0.661	2.4		1.71	0.65	1.35	50	2.4	80
18.6	5.03	14.3	2.39	0.84	0.346	1.48		0.41	0.7	0.43			
25.4	7.2	24.7	3.69	1.26	0.609	2.36		1.72	0.65	0.71			
24.8	7.29	20.3	3.67	1.24	0.611	2.26		2.05	0.63	0.93			
22.3	7.19	13.3	3.37	1.18	0.552	2.02			0.81				
32.5	6.03	11.6	2.75	0.94	0.46	1.59				1.32			
16.2	19.63	49.8	7.19	1.98	1.025	3.47		3.27	2.86	0.53			
18.1	22.47	53.1	7.83	1.97	1.144	3.83		3.57	2.15				
17	25.01	53.4	8.88	2.32	1.269	4.73		3.93	4.15	0.51			
37.4	5.9	15.7	3.4	1.08	0.516	1.7		1.08	0.42	2.72		5.9	80
26.4	15.6	43.6	6.4	1.9	0.98	3.1							
24.4	17.6	46.9	7.17	2.17	0.987	3.34	0.48	2.87	1.71	1.48	76	4.8	92
28	9.6	24.8	4.47	1.5	0.689	2.3	0.33	1.34	1.01	2.34	177		

with a Multi Collector ICP-MS at the Open University, UK. $^{230}Th/^{232}Th$ ratio for KH78001 is taken from Chabaux (1993). The $^{234}U/^{238}U$ ratios have been measured by TIMS.

Elemental separations followed the procedures described by Claude-Ivanaj (1997) for radium, and Bourdon et al. (1999a) for protactinium. The chemical method used for U and Th was developed by Manhès (1981). All chemical separations are based on liquid-solid chromatographic extraction methods, using ion exchange resins. Typical blanks are 0.1 fg for Ra, <1 fg for Pa, 15 pg for Th and 5 pg for U. Thorium and U concentrations were measured on a VG 354 mass spectrometer; $^{230}Th/^{232}Th$ (for TIMS determinations), $^{234}U/^{238}U$ ratios, Ra and Pa concentrations on a Finnigan MAT 262. External analytical uncertainty is ≈1% for Ra, <1% for U, Th abundances and ~1.5% for Pa. It is <1% for $^{230}Th/^{232}Th$ ratios, except for KH78001 and X177/83 where external analytical uncertainty is ~ 2%.

Measurements of standards or rocks previously analyzed in the literature were also performed (Table 3). AThO, an Icelandic rhyolite obsidian, was used to check U, Th and Ra abundances (Peate et al., 2001) and Hek-8, an Icelandic dacite, to check U, Th and Pa concentrations (Sigmarsson et al., 1992; Pickett and Murrell, 1997). $^{230}Th/^{232}Th$ and $^{234}U/^{238}U$ ratio analyses were checked using standards Th S1 (Claude-Ivanaj et al., 1998) and NBS 960 (Cheng et al., 2000), respectively. All the standard measurements are within a 1% range, at the 2σ level, from the published values for U, Th and Ra abundances, 2% for Pa, <1% for $^{234}U/^{238}U$ ratios and $^{230}Th/^{232}Th$ ratios

Table 2. Radiogenic isotope data for Central Kamchatka Depression lavas.

Sample	$^{143}Nd/^{144}Nd$	$^{87}Sr/^{86}Sr$	$^{206}Pb/^{204}Pb$	$^{207}Pb/^{204}Pb$	$^{208}Pb/^{204}Pb$	$^{187}Os/^{188}Os$
Klyuchevskoy						
Basalt						
K77381	0.51312 ± 2	0.70350 ± 2	18.271 ± 16	15.478 ± 17	37.909 ± 55	0.142 ± 0.5
KH78001	0.51310 ± 2	0.70350 ± 2	18.291 ± 14	15.480 ± 15	37.908 ± 53	
K56P66	0.51308 ± 2	0.70365 ± 2	18.292 ± 15	15.460 ± 16	37.777 ± 54	0.203 ± 2
Plosky Tolbachik						
Basalt						
PT33-1/82	0.51308 ± 1	0.70353 ± 2	18.294 ± 13	15.471 ± 15	37.846 ± 52	0.222 ± 5
PT10-1/82	0.51311 ± 1	0.70335 ± 2	18.193 ± 13	15.482 ± 16	37.858 ± 54	
GTFE						
Basalt						
T1475/1975	0.51310 ± 2	0.70334 ± 2	18.284 ± 13	15.479 ± 15	37.805 ± 52	0.175 ± 1
PT30-4/1976	0.51310 ± 2	0.70334 ± 2	18.256 ± 16	15.471 ± 21	37.814 ± 57	0.147 ± 1

Osmium isotopes data from Alves et al. (2002). GTFE: Great Tolbachik Fissural Eruption (1975–1976).

measured by MC ICP-MS, and 1.3% for $^{230}Th/^{232}Th$ ratios measured by TIMS.

5. RESULTS

The results of our analyses are reported in Table 3. ^{226}Ra concentrations range between 199 and 896 fg/g. ^{231}Pa abundances show less variability (183–570 fg/g). Uranium and Th contents range from 0.337 to 1.36 and 0.500 to 2.31 ppm, respectively. All these values are within the range found for arc magmas worldwide (Gill and Williams, 1990; Hawkesworth et al., 1997, and references therein for U, Th; Turner et al., 2001, for Ra; and Pickett and Murrell, 1997; Bourdon et al., 1999b, for Pa). It is also similar to the range of available data for Klyuchevskaya group volcanoes (Turner et al., 1998, 2001).

Abundances of U, Th and ^{231}Pa are all positively correlated showing that they behave as incompatible elements. The ^{226}Ra contents show weaker correlation with the other elements probably because ^{226}Ra decay may have degraded any preexisting correlation with this element.

The ($^{230}Th/^{238}U$) activity ratios (in this article, all isotopic ratios in parentheses denote activity ratios) display values both lower and higher than unity (0.92–1.12), similarly to previous data on Klyuchevskaya group volcanoes (Turner et al., 1998). A ^{230}Th excess over ^{238}U is uncommon for arc lavas as they are usually characterized by either ^{238}U excess over ^{230}Th, or close to secular equilibrium (Allègre and Condomines, 1982). Few arcs (Central America, Chile) show substantial excess of ^{230}Th over ^{238}U (Reagan and Gill, 1989; Reagan et al., 1994; Sigmarsson et al., 1998; Clark et al., 1998; Bourdon et al., 2000). This has been interpreted to result from melting of either the subducted oceanic crust or lower continental crust in the presence of residual garnet. This point will be discussed further.

The ($^{226}Ra/^{230}Th$) ratios are characterized by a wide range (1.00–2.72), which is comparable to previous data for Tolbachik lavas (Turner et al., 2001) and to the global range for arcs (0.873–8.0; Gill and Williams, 1990; Hoogewerff et al., 1997; Turner et al., 2000, 2001). As our samples were all erupted within the last century, no time correction was needed for these ratios.

The ($^{231}Pa/^{235}U$) ratios range from 1.22 to 1.56. This is also comparable with the range reported for arc volcanics (Pickett and Murrell, 1997; Bourdon et al., 1999b). The ($^{230}Th/^{232}Th$) activity ratios are remarkably high, even compared with other arc lavas (e.g., Hawkesworth et al., 1997), with values as high as 2.25. It is also striking that the range in ($^{230}Th/^{232}Th$) ratios (1.83–1.98) is relatively narrow for the Tolbachik and Klyuchevskoy lavas. The samples from Tolbachik analyzed in Turner et al. (1998) also plot within this range.

Another important observation is that parent-daughter activity ratios are correlated with MgO (Fig. 3). The most primitive lava (high MgO content) is characterized by high ($^{226}Ra/^{230}Th$), ($^{231}Pa/^{235}U$) ratios, and ($^{230}Th/^{238}U$) <1, whereas the most differentiated lava displays ($^{226}Ra/^{230}Th$) in secular equilibrium, lower ($^{231}Pa/^{235}U$) ratio and ($^{230}Th/^{238}U$) >1.

Finally, ($^{234}U/^{238}U$) activity ratios are all in secular equilibrium or very close to as they range from 0.98 to 1.01 ± 0.01. It suggests that ^{234}U and ^{238}U have not been recently fractionated by chemical weathering or hydrothermal circulation.

6. ORIGIN OF U-SERIES DISEQUILIBRIA

6.1. Controls on ^{238}U-^{230}Th-^{226}Ra and ^{235}U-^{231}Pa Fractionation

In this section, we examine mostly from a qualitative viewpoint what might explain the observed U-series disequilibrium in the CKD arc lavas. The first striking feature of our new ^{230}Th-^{238}U data is that for most lavas, ($^{230}Th/^{238}U$) ratios are >1. In the case of Andean austral volcanic zone in southern Chile, ^{230}Th excesses in arc lavas have been explained by slab melting (Sigmarsson et al., 1998). On the other hand, crustal assimilation and melting appears as another possible mechanism to account for this observation, as in the case of northern Chile (Bourdon et al., 2000). It is interesting to note that samples with ($^{230}Th/^{238}U$) >1 are high-alumina basalts or andesites, whereas those with ($^{230}Th/^{238}U$) <1 are exclusively high-magnesia basalts (see Fig. 2b). Thus, it seems that there could be a link between the processes fractionating Th-U in the subduction zone and the origin of high-alumina andesites and high-magnesia basalts (see discussion below).

Our dataset displays high ($^{230}Th/^{232}Th$) and ($^{238}U/^{232}Th$) ratios (Fig. 4). Two reasons may explain this observation: (1) the source of magmas could be a mixture between a N-MORB mantle and subducted sediments with low Th/U ratios (and hence high $^{230}Th/^{232}Th$) such as carbonates, or (2) the source is

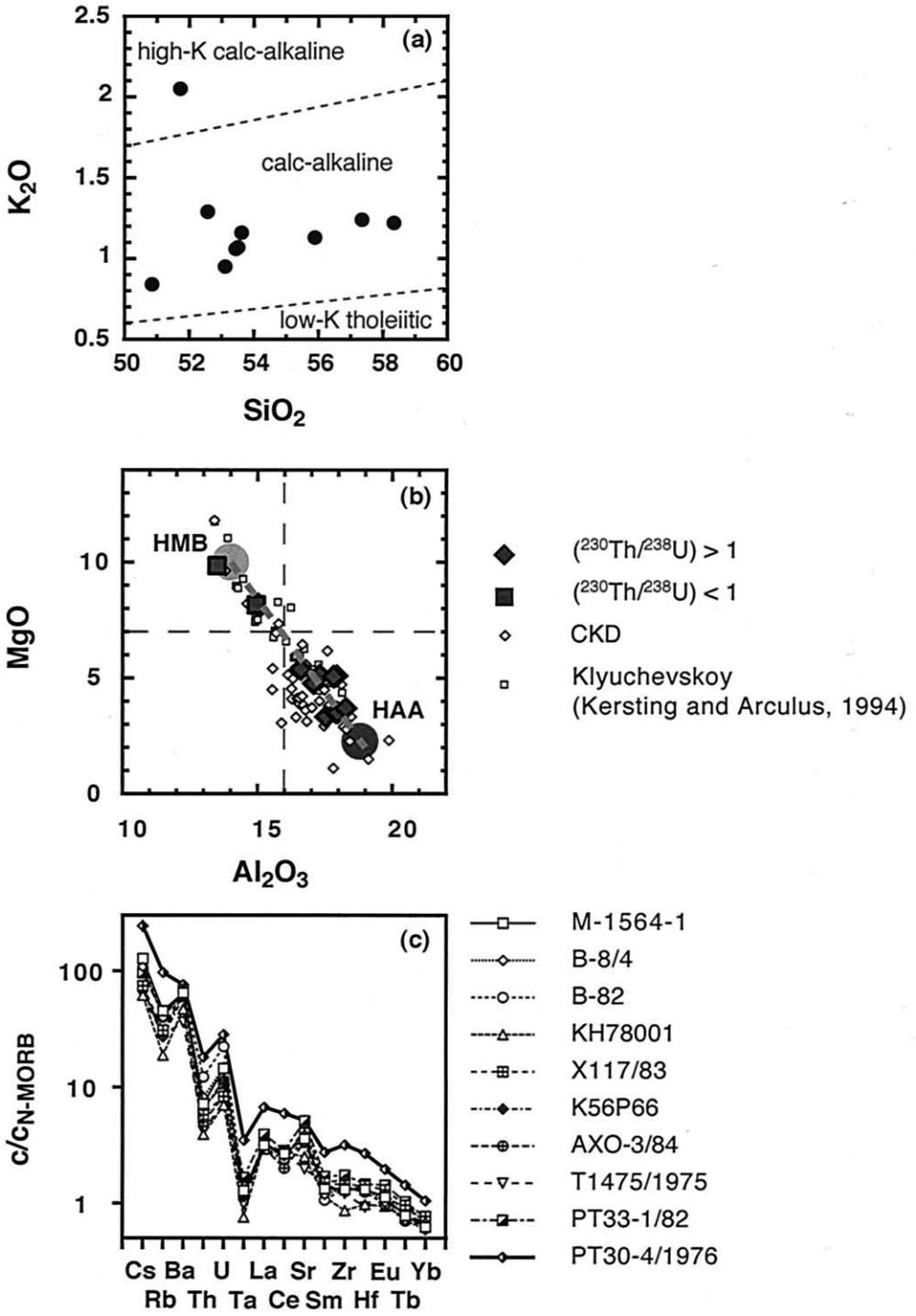

Fig. 2. (a) K_2O vs. SiO_2 contents (wt.%). The only samples reported in this diagram were analyzed for U-series. They are all medium-K calc-alkaline lavas except for one sample (PT30-4/1976), which plots in the high-K calc-alkaline field. (b) MgO vs. Al_2O_3 contents (wt.%). Large diamonds are samples exhibiting $(^{230}Th/^{238}U) > 1$, and large squares, $(^{230}Th/^{238}U) < 1$. Small diamonds are samples from this study that have not been analyzed for U-series. Small squares are data from Kersting and Arculus (1994). Horizontal and vertical dashed lines define high-magnesia basalt (upper-left quarter) and high-alumina basalt and andesite fields (lower-right quarter). Note that samples with ^{230}Th excess are located only in the high-alumina field, and samples with ^{238}U excess are in the high-magnesia field. The correlation between MgO and Al_2O_3 can be reproduced by a mixing line (grey dashed line) connecting a high-magnesia basalt (HMB) end-member with a high-alumina andesite (HAA) end-member (large dots; see Table 4 for end-member compositions). (c) Trace element patterns where concentrations are normalized to abundances in N-MORB (Hofmann, 1988) for samples analyzed for U-series. PT30-4/1976 displays a pattern shifted upward compared to other samples.

Table 3. U-series data for Central Kamchatka Depression lavas.

Sample	Th (ppm)	U (ppm)	^{226}Ra (fg/g)	Pa (fg/g)	(^{230}Th/^{238}U)	(^{226}Ra/^{230}Th)	(^{231}Pa/^{235}U)	(^{234}U/^{238}U)	(^{230}Th/^{232}Th)
BEZYMIANNY									
Basic andesite									
M-1564-1	1.100	0.696	278.7 ± 4.4	298.4 ± 3.7	1.058 ± 0.001	1.097 ± 0.017	1.314 ± 0.016	1.010 ± 0.009	2.020 ± 0.001*
Acid andesite									
B-8/4	1.127	0.773	340.8 ± 5.9	349.4 ± 2.3	1.089 ± 0.040	1.173 ± 0.048	1.384 ± 0.009	1.006 ± 0.007	2.253 ± 0.083*
Replicate	1.139	0.771	339.3 ± 3.1						
B-82	1.563	0.860	330.5 ± 2.1	366.3 ± 5.2	1.119 ± 0.001	0.995 ± 0.006	1.304 ± 0.018	1.001 ± 0.010	1.857 ± 0.002#
Klyuchevskoy									
Basalt									
KH78001	0.500	0.337	277.1 ± 3.9		0.918 ± 0.042	2.615 ± 0.106			1.870 ± 0.040*
AXO-3/84	0.725	0.451	261.5 ± 2.1	196.7 ± 2.4	1.023 ± 0.002	1.642 ± 0.014	1.336 ± 0.016	0.981 ± 0.011	1.920 ± 0.003#
X117/83	0.739	0.450	239.6 ± 2.4	195.3 ± 2.0	1.029 ± 0.019	1.499 ± 0.031	1.328 ± 0.014	0.996 ± 0.007	1.892 ± 0.035*
Replicate	0.732	0.448	242.4 ± 8.1		1.043 ± 0.014	1.516 ± 0.071		0.982 ± 0.036	1.926 ± 0.025*
K56P66	0.705	0.452	359.0 ± 1.5	211.3 ± 1.9	1.010 ± 0.001	2.279 ± 0.010	1.432 ± 0.013	0.994 ± 0.010	1.954 ± 0.003#
Plosky Tolbachik									
Basalt									
PT33-1/82	0.848	0.514	198.9 ± 2.2	205.0 ± 5.7	1.082 ± 0.001	1.035 ± 0.011	1.220 ± 0.034	1.010 ± 0.022	1.980 ± 0.003#
GTFE									
Basalt									
T1475/1975	0.539	0.360	325.5 ± 1.9	183.4 ± 3.9	0.961 ± 0.001	2.724 ± 0.016	1.560 ± 0.033	0.999 ± 0.010	1.938 ± 0.001#
PT30-4/1976	2.307	1.358	890.1 ± 7.9	569.8 ± 5.1	1.032 ± 0.003	1.840 ± 0.017	1.284 ± 0.011	1.010 ± 0.012	1.834 ± 0.005*
Replicate			895.8 ± 13.0	561.7 ± 8.3					

		Th (ppm)	U (ppm)	^{226}Ra (fg/g)	Pa (fg/g)	STANDARD		(^{230}Th/^{232}Th)	(^{234}U/^{238}U)
AThO	Standard	7.44	2.26	845 ± 8		ThS1	Standard	5.491 ± 11 × 10^{-6}	
	(n = 2; 2σ)	7.43 ± 0.03	2.23 ± 0.05	841.7 ± 1.4		TIMS	(n = 4; 2 σ)	5.551 ± 140 × 10^{-6}	
Hek-8	Standard	7.74	2.32		900.0	MC ICP-MS	(n = 9; 2 σ)	5.497 ± 22 × 10^{-6}	
	(n = 2; 2 σ)	7.75 ± 0.07	2.31 ± 0.01		881.7 ± 5.6	NBS960	Standard		5.267 × 10^{-5}
							(n = 5; 2 s. d.)		5.307 ± 64 × 10^{-5}

Parentheses denote activity ratios. ^{230}Th/^{232}Th have been measured by TIMS (*) or MC ICP-MS (#). (^{230}Th/^{232}Th) value for KH78001 is taken from Chabaux (1993). Standard ^{230}Th/^{232}Th value for ThS1, and ^{234}U/^{238}U for NBS960 are taken, respectively, from Claude-Ivanaj et al. (1998) and Cheng et al. (2000). GTFE: Great Tolbachik Fissural Eruption.

an N-MORB mantle that has been enriched in U over Th via a slab fluid, sufficiently long ago to produce high (^{230}Th/^{232}Th) ratios by radioactive decay. The first hypothesis can be precluded since, to produce the observed (^{230}Th/^{232}Th) ratios, 7 wt.% of carbonates are required in the source of the CKD lavas, and such large amount of carbonate would shift ^{87}Sr/^{86}Sr ratios to much higher values (0.706) than those observed (~0.703). Moreover, there is no substantial amount of carbonates in the sediment pile drilled in ODP sites 881 to 884, which are thought to be representative of sediments subducted beneath the Kamchatka arc (Rea, 1993). It is more likely that, as previously suggested by Turner et al. (1998), the source has been enriched in U over Th by a slab-derived fluid sufficiently long ago to produce high (^{230}Th/^{232}Th) ratios. Turner et al. (1998) have defined a lower age for this event of 150 ka. Additionally, ^{238}U excesses are probably linked to fluid addition as (^{230}Th/^{238}U) ratios are negatively correlated with Sr/Th and Rb/Th ratios (Figs. 5a and 5b). As U, Rb and Sr are mobile elements while Th is not, fluid will be characterized by low (^{230}Th/^{238}U) and high Sr/Th and Rb/Th ratios.

All the samples are characterized by (^{231}Pa/^{235}U) >1. This has been observed in other arcs and is believed to be a consequence of the greater incompatibility of ^{231}Pa over ^{235}U during partial melting in presence of residual clinopyroxene ± garnet (Pickett and Murrell, 1997; Fig. 6a). In addition, it has been shown that melting by equilibrium porous flow can account for the observed (^{231}Pa/^{235}U) ratios in Kermadec arc magmas (Bourdon et al., 1999b). We tested below if this process could also explain Kamchatka (^{231}Pa/^{235}U) ratios, as they show a range similar to the Kermadec data.

The ^{226}Ra-^{230}Th disequilibria found in CKD lavas cannot be explained by surficial processes such as chemical weathering, for several reasons: (1) chemical weathering would produce a deficit in mobile elements in the rock. As Ra is more fluid-mobile than Th, (^{226}Ra/^{230}Th) ratios <1 would be expected, which is in contrast with what is observed. (2) Pineau et al. (1999), on the basis of oxygen and hydrogen isotopes, have demonstrated that all our samples are fresh and free from any chemical alteration. (3) The (^{234}U/^{238}U) activity ratios are in secular equilibrium (Table 3). If water-rock interaction had occurred, (^{234}U/^{238}U) ratios <1 would be expected, as during chemical weathering, ^{234}U is lost more readily than ^{238}U.

Fractional crystallization could in principle fractionate Ra from Th but, as they are both very incompatible elements, this fractionation would be too low to account for the high (^{226}Ra/^{230}Th) ratios observed. Additionally, as the most magnesian lavas exhibit the highest (^{226}Ra/^{230}Th), fractionation must have taken place before crystallization.

The ^{226}Ra excesses in volcanic rocks have often been explained by partial melting because radium is more incompatible than thorium during this process (e.g., Gill and Williams, 1990). Furthermore, as high (^{226}Ra/^{230}Th) ratios are associated

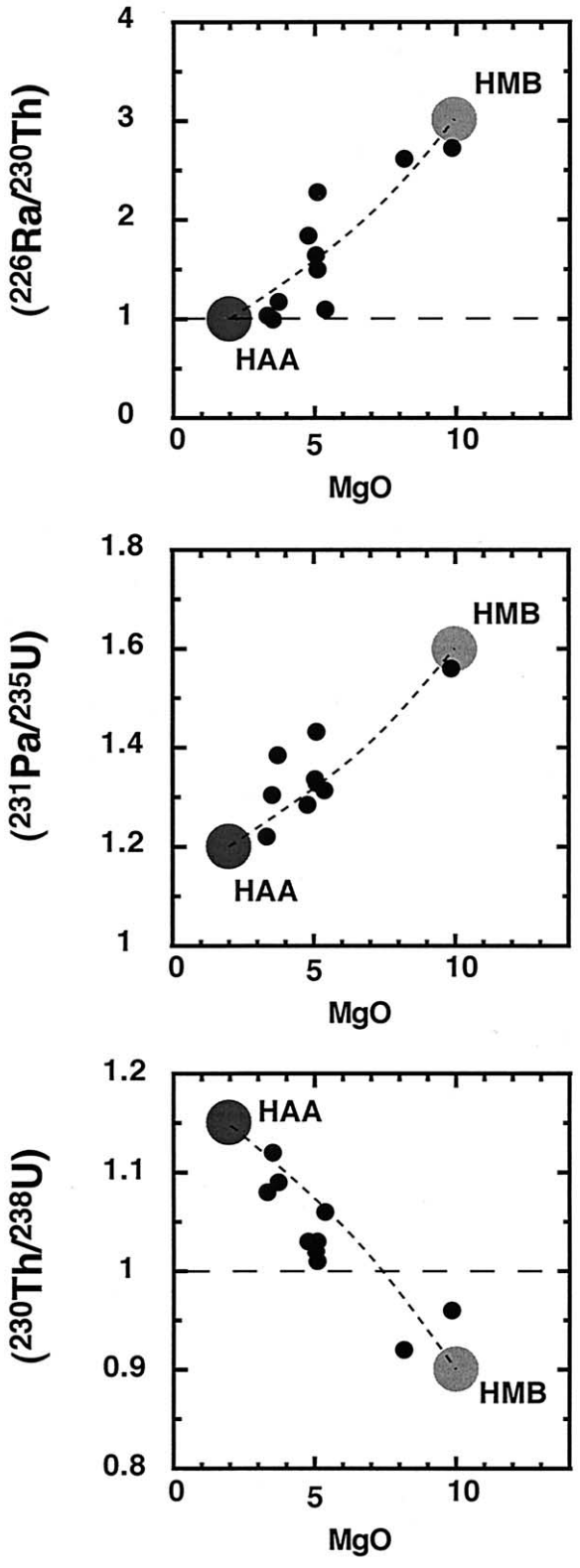

Fig. 3. Daughter/parent activity ratios vs. MgO content (wt.%). (a) (^{226}Ra/^{230}Th), (b) (^{231}Pa/^{235}U) and (c) (^{230}Th/^{238}U) activity ratios. The dashed curves are mixing curves between high-alumina andesite (HAA) and high-magnesia balsalt (HMB) end-members (large dots; composition of end-members used for calculation is reported in Table 4). Horizontal dashed lines are for secular equilibrium (equilines).

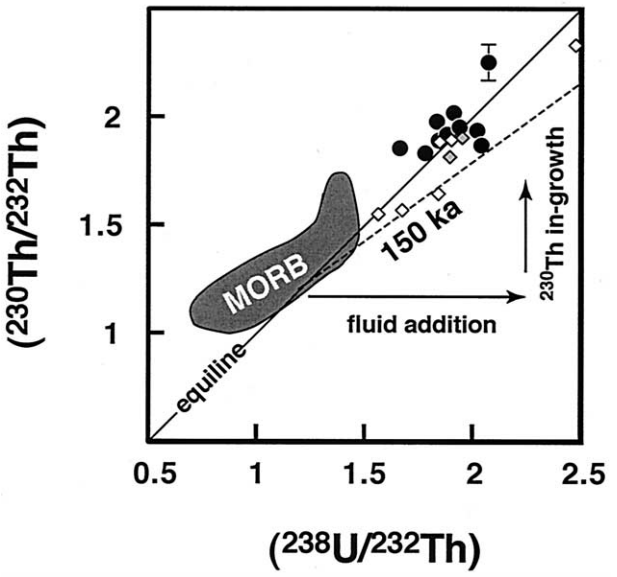

Fig. 4. ^{230}Th-^{238}U isochron diagram for CKD lavas. Data from this study are shown as black dots; diamonds are CKD data from Turner et al. (1998). The MORB field is from Bourdon et al. (1996). Note the high (^{230}Th/^{232}Th) ratios and that most points are located to the left of the equiline. Data from Turner et al. (1998) for the same volcanoes as those studied here (Tolbachik; grey diamonds), show a similar range in (^{230}Th/^{232}Th) when compared with our data. Turner et al. (1998) have interpreted the ^{230}Th-^{238}U characteristics as the result of a 150-ka-old fluid addition to the wedge.

with (^{231}Pa/^{235}U) ratios >1 (Fig. 6a), it could be inferred that this process is indeed responsible for ^{226}Ra excesses, as the solid/melt partition coefficients are ordered as follows: $D_{Ra} < D_{Th}$ and $D_{Pa} < D_{U}$. On the other hand, (^{230}Th/^{238}U) <1, associated with the highest (^{226}Ra/^{230}Th), is not a typical melting signature (Fig. 6b).

Another possibility that needs to be considered is that Ra-Th disequilibrium results from fluid addition due to dehydration of the subducted slab. If the fluid addition event that produced the large (^{230}Th/^{232}Th) ratios and ^{238}U excess in the Kamchatka lavas has occurred at least 150 ka ago (Turner et al., 1998), the same event cannot account for the observed (^{226}Ra/^{230}Th) ratios since any ^{226}Ra-^{230}Th disequilibrium decays within 8 ka.

It has been argued that the correlation between (^{226}Ra/^{230}Th) and Ba/Th in other arcs is an indication that ^{226}Ra excesses reflect a fluid contribution (Turner et al., 2000, 2001). In the case of Kamchatka arc, (^{226}Ra/^{230}Th) and Ba/Th ratios are also correlated, except for two samples (not shown). One of them (PT30-4/1976) always displays very different incompatible element concentrations and it is argued above that it may have had a different history compared with the other samples. Plotting (^{226}Ra/^{230}Th) vs. Sr/Th or Rb/Th shows positive trends where the highest ^{226}Ra excess is associated with the strongest fluid signature (high Sr/Th, Rb/Th ratios; Figs. 5c and 5d). Thus, ^{226}Ra excesses must be associated with fluid addition. Melting possibly produces some ^{226}Ra excess but cannot account for the positive correlations with Sr/Th and Rb/Th. As Sr is more compatible than Th, which is itself more compatible than Ra, during melting, Sr/Th should be negatively correlated to (^{226}Ra/^{230}Th). Moreover, Rb/Th will not fractionate for a

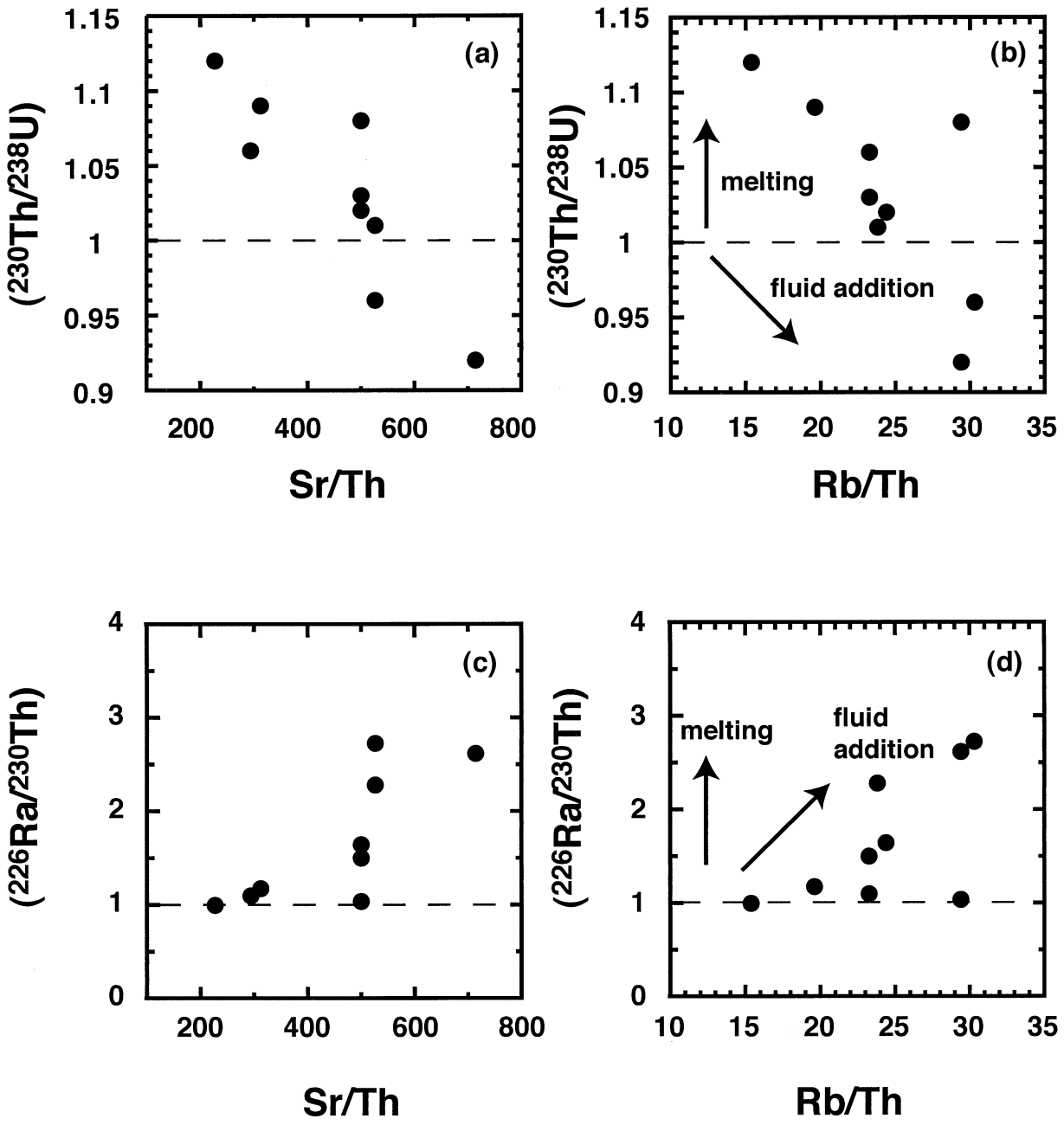

Fig. 5. (^{230}Th/^{238}U) ratios vs. Sr/Th (a), Rb/Th (b) and (^{226}Ra/^{230}Th) vs. Sr/Th (c) and Rb/Th (d). Arrows show the effects of melting or fluid addition on magma compositions. Data for PT30-4/1976 are not shown as this sample exhibit very different incompatible trace element content, compared with the other samples, and is believed to have had a different history. The strongest fluid signature (high Rb/Th and Sr/Th ratios) is associated with ^{238}U and ^{226}Ra excesses over ^{230}Th, and suggests that these disequilibria are fluid-derived. Horizontal dashed lines are equilines.

degree of partial melting >1%. A possible scenario would be that there have been at least two events of fluid addition: the first one would have occurred >150 ka ago and account for the high (^{230}Th/^{232}Th) ratios (Fig. 4). The second event would have occurred at most a few thousand years before eruption and produced the ^{226}Ra excesses and possibly some of the ^{238}U excess. In what follows, we also consider the case of multiple fluid addition events (see below). However, as mentioned above, (^{226}Ra/^{230}Th) is positively correlated with (^{231}Pa/^{235}U) and this cannot be explained by a fluid contribution only.

Consequently, the trends between activity ratios cannot be explained by a single process as: (1) the positive correlation between (^{226}Ra/^{230}Th) and (^{231}Pa/^{235}U) would suggest a melting trend (Fig. 6a); (2) while the negative trend between (^{226}Ra/^{230}Th) and (^{230}Th/^{238}U) is better explained by a fluid addition (Fig. 6b); this is supported by the positive correlations between

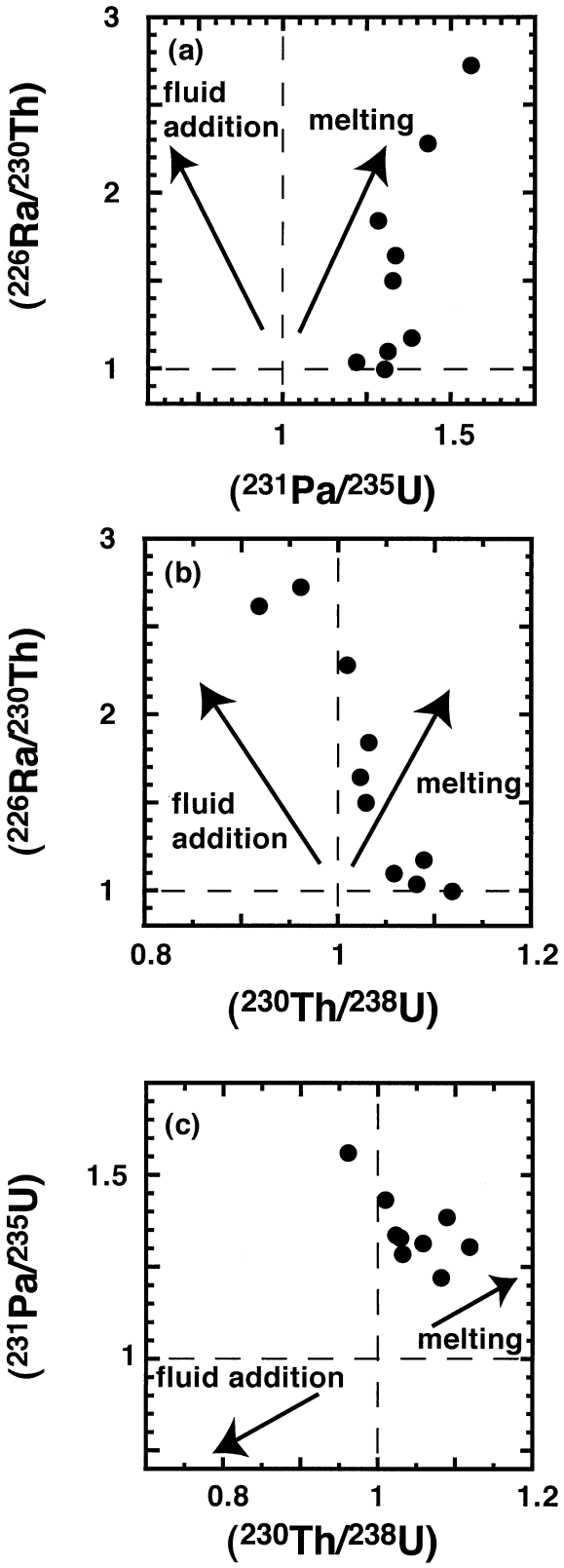

Fig. 6. Binary diagrams of daughter/parent activity ratios. Arrows show the effects on uranium series of melting and fluid addition. None of these processes can account alone for the observed trends. Horizontal and vertical dashed lines are equilines.

^{226}Ra excess and Sr/Th and Rb/Th ratios); and (3) the (^{231}Pa/^{235}U) vs. (^{230}Th/^{238}U) negative trend cannot be explained neither by melting nor by fluid addition (Fig. 6c). It seems thus unlikely that a single process can explain the U-series data for the Central Kamchatka Depression.

6.2. Evidence for Mixing Between Two Magma Types

As suggested above, there is no simple model that combines fluid addition and melting to provide a good explanation for observed trends in U-series disequilibria. A previous study of Klyuchevskoy has suggested that the major element characteristics of lavas from this volcano could result from mixing between high-alumina and high-magnesia basalts (Kersting and Arculus, 1994). Indeed, correlations between MgO and Al_2O_3 contents for our CKD data and data from Kersting and Arculus (1994) could be explained by mixing between a high-magnesia basalt (HMB) end-member with MgO = 10 wt.% and Al_2O_3 = 14 wt.%; and a high-alumina andesite (HAA) end-member with MgO = 2 wt.% and Al_2O_3 = 19 wt.% (Fig. 2b). In the case of our data set, high-alumina andesite end-member is preferred over a high-alumina basalt as a silica content of 60 wt.% is required for this end-member. Mixing hypothesis is supported by petrological observations as disequilibrium features are preserved in the phenocrysts of hybrid basalts, which have intermediate composition between high-alumina and high-magnesia basalts (Kersting and Arculus, 1994). If we consider that the end-members are characterized by distinctive U-series signatures, then the relationships between activity ratios and MgO content can easily be explained by mixing (Fig. 3; see Table 4 for end-member compositions). The same mixing curves fit the data in diagrams where each activity ratio is plotted versus another (Fig. 7). Consequently, mixing between HMB and HAA with different U-series characteristics, appears to be the simplest explanation for the relationships between ^{238}U-^{230}Th-^{226}Ra and ^{235}U-^{231}Pa disequilibria. This hypothesis is also supported by trace element and isotope data such as La/Yb and ^{187}Os/^{188}Os ratios which all correlate negatively with MgO content (Fig. 8). As crystallization cannot extensively fractionate La/Yb ratio and produce higher ^{187}Os/^{188}Os ratios in low MgO lavas, mixing between two end-members with different origins is more likely to explain these relationships. The HAA end-member has higher La/Yb and ^{187}Os/^{188}Os ratios than the HMB end-member. On the other hand, no relationship is observed between Nd, Sr and Pb isotopes and MgO content. As the samples display nearly constant compositions for these isotopes, both end-members must have similar Nd, Sr and Pb isotopes composition.

The distinct U-series signatures for HMB and HAA end-members still need to be explained. In the following discussion, we examine some quantitative models for explaining the U-series disequilibria for Central Kamchatka Depression lavas, and we shall attempt to reproduce HMB and HAA end-member compositions.

7. QUANTITATIVE MODELS FOR U-SERIES DISEQUILIBRIA IN CKD ARC LAVAS

As a first step, we propose models for explaining the HMB end-member composition. This end-member displays ^{238}U and

Table 4. High-Magnesia Basalt (HMB) and High-Alumina Andesite (HAA) end-members composition.

	SiO_2	Al_2O_3	MgO	Th	U	($^{230}Th/^{238}U$)	($^{231}Pa/^{235}U$)	($^{226}Ra/^{230}Th$)
HMB	50	14	10	0.500	0.300	0.9	1.6	3
HAA	60	19	2	1.300	0.700	1.15	1.2	1

Silica, alumina and magnesia contents in wt.%. Thorium and U contents in ppm. Parentheses denote activity ratios.

^{226}Ra excesses together with high Ba/Th, Sr/Th and Rb/Th ratios, which are typical of a fluid signature. It is also characterized by MORB-like Pb and Nd isotopic compositions. As U, Ra, Ba, Sr and Rb are mobile elements, unlike Th, HMB end-member shows the characteristics of a magma derived from mantle that has been metasomatized by fluids. In the following section, three quantitative models for slab dehydration are tested.

Firstly, we examine a model of discrete fluid addition as has been proposed in the literature (Turner et al., 1996, 1998; Elliott et al., 1997; Turner and Hawkesworth, 1997). Secondly, it has also been suggested, based on ^{226}Ra-^{230}Th-^{238}U systematics of the Tonga-Kermadec arc, that fluid addition is more likely to occur as a two-step process (Turner et al., 2000; Fig. 9a). This model is also tested for Kamchatka. Thirdly, a model of continuous dehydration of the slab is considered. It is worth testing if a continuous supply of fluid to the wedge can account for U-series characteristics of arc magmas as numerous petrologic studies have shown that several hydrated mineral phases in the slab are expected to be destabilized and to supply fluids to the mantle wedge (Kushiro et al., 1967; Lambert and Wyllie, 1972; Green, 1973; Millhollen et al., 1974; Delany and Helgeson, 1978; Wyllie, 1979; Basaltic Volcanism Study Project, 1981; Bohlen et al., 1983; Tatsumi and Nakamura, 1986; Iwamori, 1998; Schmidt and Poli, 1998). This suggests that fluid addition may occur through multiple events or even continuously (Ishikawa and Nakamura, 1994; Ishikawa and Tera, 1997; Shibata and Nakamura, 1997; Schmidt and Poli, 1998).

We have considered two versions of the continuous dehydration. In the first model, termed continuous flux melting, continuous fluxing of the wedge by fluids is assumed to induce melting of the mantle wedge instantaneously such that a small batch of melt is produced each time that a fraction of fluid is added (Fig. 9b). This model is fully described in Bourdon et al. (in press) and tested here for Kamchatka data. In the second model, the slab fluid is also continuously added to the wedge, but in this case, melting only occurs once the wet peridotite reaches its solidus, at a greater depth, where the continuous dehydration process ends (Fig. 9c).

The HMB end-member also shows ^{231}Pa excesses. It has been argued that such a signature can only result from melting. We have thus considered both dynamic melting and equilibrium transport melting as alternatives to the continuous flux melting model.

7.1. Fractionation in U-Series Due to Discrete Fluid Additions

The U-Th disequilibrium data for the Kamchatka lavas suggest that the source of the lavas has been metasomatized >150 ka before eruption. In contrast, the Ra-Th disequilibrium data that correlate with indices of fluid addition indicate a recent fluid addition (less than a few thousand years). Consequently, an explanation for this apparent paradox could be that there are (at least) two episodes of fluid addition as has been proposed for the Tonga-Kermadec arc (Turner et al., 2000). In their model, Turner et al. (2000) propose that a first U, Ra-rich fluid is added to the wedge, followed by a second fluid addition, 60 ka later and shortly before eruption, containing only ^{226}Ra produced by decay of ^{230}Th retained in the slab. Indeed, as U is believed to be very mobile in oxidizing conditions, they suggest that most of the available U in the slab will be mobilized during the first event. A small fraction of U could be added by the second fluid and will have little effect on the U budget of the metasomatized mantle.

In the case of Kamchatka, it is more likely that the time lag between the two events is close to 150 ka to produce high ($^{230}Th/^{232}Th$) and low ^{238}U excess. Using the two-step dehydration model from Turner et al. (2000), activity ratios have been calculated as a function of time. After the first dehydration event, most ^{238}U is removed from the slab. Thus, ^{230}Th is no longer supported by its parent. It is therefore critical to assess whether significant ^{226}Ra excess can be produced during the second dehydration. As a first step, we have used solid/fluid partition coefficients similar to those used in Turner et al. (2000). Clinopyroxene/fluid for a 5-M (Na,K)Cl fluid from Keppler (1996) and mineral/melt partition coefficients (LaTourette et al., 1993; Lundstrom et al., 1994) are used to calculate each mineral/fluid partition coefficients. If one assumes that the slab is composed of 50% garnet and 50% clinopyroxene (cpx), the following bulk solid/fluid partition coefficients for U, Th and Ra, respectively, are found: Df_U = 0.024, Df_{Th} = 0.14 and Df_{Ra} = 0.001 (partition coefficient for Ra is taken to be similar to Ba). The fraction of fluid extracted during the first and second events are taken to be 2.5 and 0.5%, respectively. The resulting ($^{226}Ra/^{230}Th$) ratios are lower than those observed in HMB, after the second fluid addition.

However, if U is assumed to be less mobile than expected based on the Keppler (1996) experiments, it is possible to reproduce HMB activity ratios using the input data given in Table 5a. The results are shown in Figure 10, which displays the various activity ratios as a function of time since the first dehydration. Initial activity ratios in the wedge, calculated after the first fluid addition, are: ($^{230}Th/^{232}Th$) = 1, ($^{230}Th/^{238}U$) = 0.45, ($^{231}Pa/^{235}U$) = 0.45 and ($^{226}Ra/^{230}Th$) = 100. After 150 ka, a second fluid containing ^{226}Ra and some ^{238}U is added. It yields the following activity ratios in the wedge: ($^{230}Th/^{238}U$) = 0.8, ($^{231}Pa/^{235}U$) = 0.9 and ($^{226}Ra/^{230}Th$) = 25. At this time, ($^{230}Th/^{232}Th$) ratio reaches the observed values as a result of ^{230}Th in-growth after the first fluid addition. Assuming less than a few thousand years for magma production and migration, ^{226}Ra decay leads to the observed ($^{226}Ra/^{230}Th$) value in

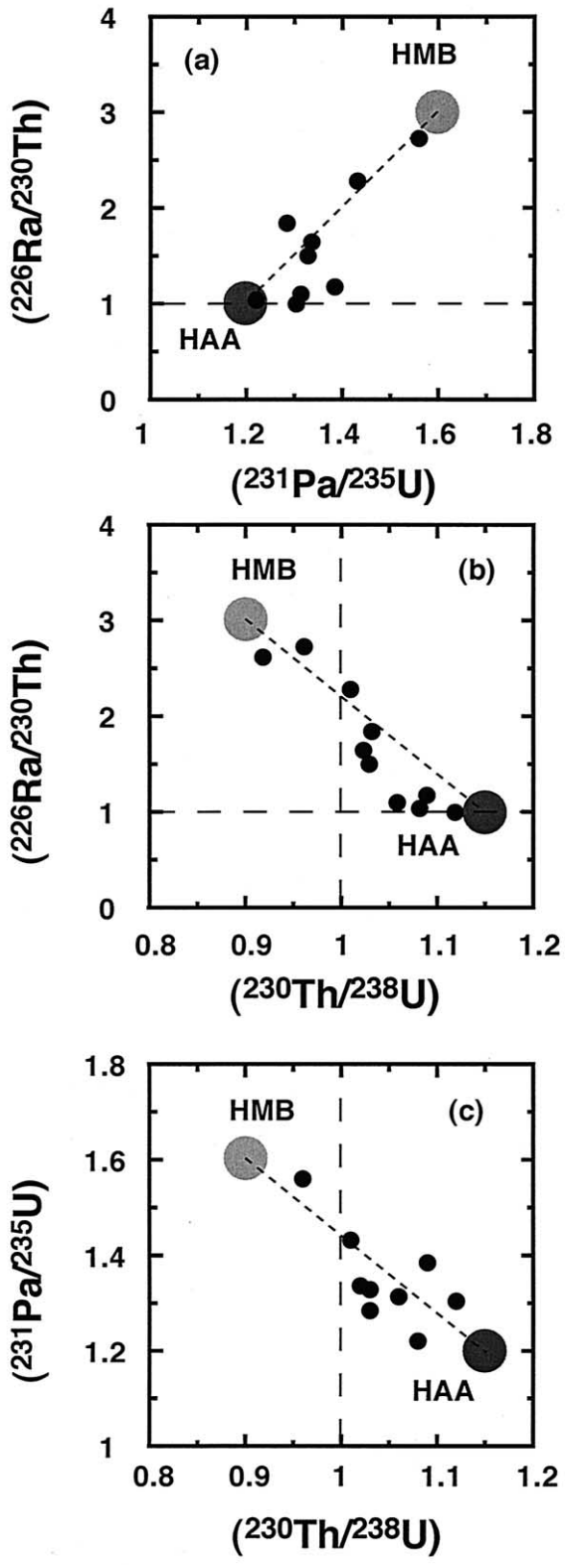

Fig. 7. Binary diagrams of daughter/parent activity ratios. Correlations can be explained by mixing (dashed curves) between high-alumina andesite (HAA) and high-magnesia basalt (HMB) end-members (large dots), as seen in Figures 2b and 3. Composition of the end-members used for calculation of mixing curves is reported in Table 4. Horizontal and vertical dashed lines are equilines.

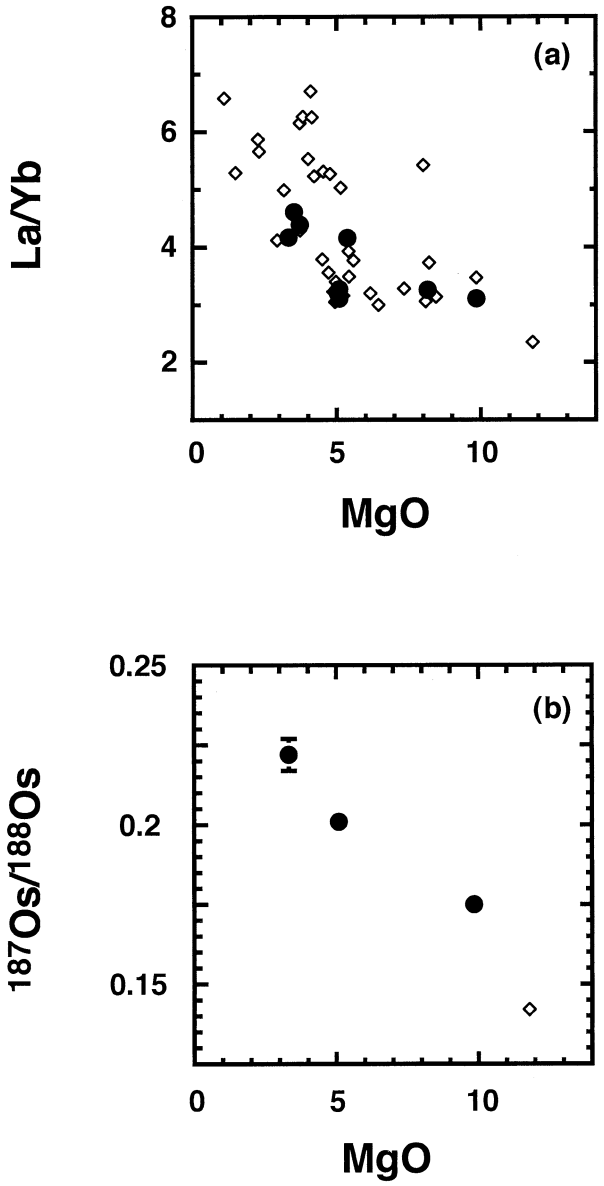

Fig. 8. La/Yb (a) and $^{187}Os/^{186}Os$ (b) ratios vs. MgO content (wt.%). Samples that have been analyzed for U-series are shown as black dots, whereas the others are represented by diamonds. Data for PT30-4/1976 are not shown as this sample exhibit very different incompatible trace elements content, compared with the other samples. These trends support a mixing hypothesis for explaining correlations between U-series disequilibria, as fractional crystallization cannot explain the differences in trace element and isotope characteristics.

the HMB end-member. This model can account for ^{238}U-^{230}Th-^{226}Ra characteristics of the HMB end-member. A melting model is then needed to explain ^{231}Pa excesses, taking into account that the source may be close to secular equilibrium for ^{235}U-^{231}Pa (see section 7.4).

7.2. Continuous Flux Melting

In this model, fluid is continuously added to the mantle wedge, which is assumed to be hot enough such that melting

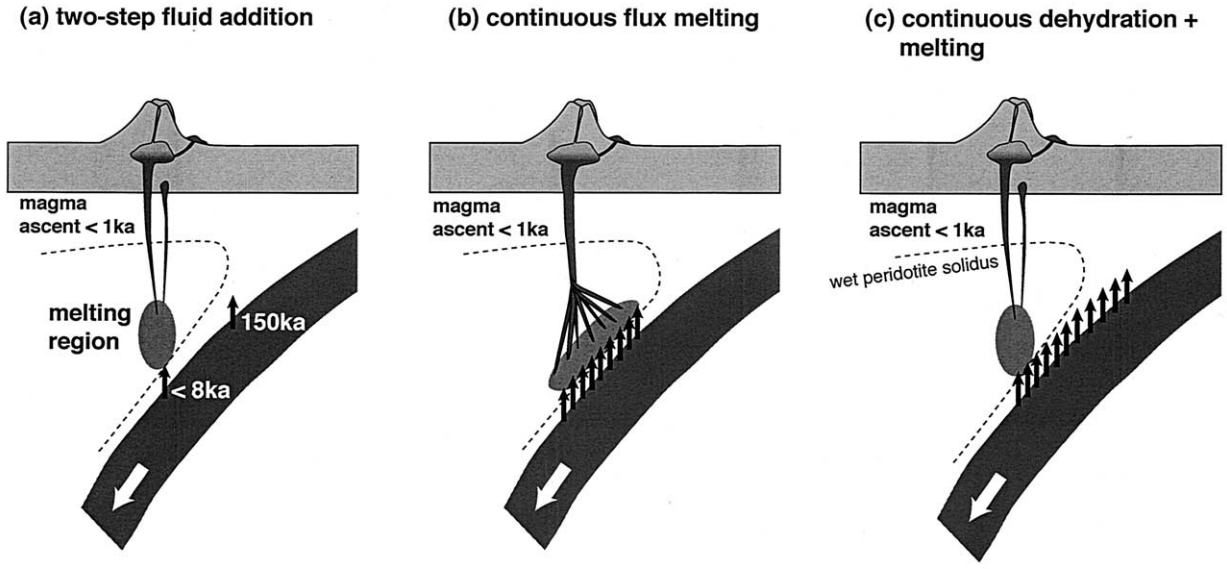

Fig. 9. Schematic diagrams for models evaluated for slab dehydration (see text for details). Vertical black arrows are dehydration events. Shaded area in the wedge is the melting region. Large white arrow shows slab subduction. In (a), numbers close to the black arrows are ages for the two dehydration events: 150 ka for the first and <8 ka for the second.

would occur instantaneously after fluid addition. In this case, melting starts with the inception of dehydration and each increment of fluid added to the wedge induces more melting (Fig. 9b). We have attempted to reproduce the composition of the HMB end-member with this scenario. The model used in this section is fully described in Bourdon et al. (in press). Here, we mostly deal with the main features and provide input parameters.

The continuous flux melting process is described by a series of time steps during which small increments of fluid are produced in the slab, added to the wedge and induce production of small batches of melt (see Fig. 9b). At each time step, the composition of the fluid is calculated assuming a batch process for dehydration. The fraction of fluid produced is determined as the total fraction of fluid extracted during continuous flux melting divided by the number of time steps. The fluid is added to the wedge and melt is produced in equilibrium within the metasomatized wedge. Similarly to the dehydration process, the degree of melting at each time step is defined as the ratio of the final degree of partial melting to the number of time steps. After magma extraction, a constant fraction of the melt remains in equilibrium with the source. Between each time step, standard decay equations are used to track the abundance of U-series nuclides both in the wedge and the oceanic crust. Once melts are extracted from all levels in the source, they are accumulated instantaneously before eruption.

The composition of accumulated melt has been calculated as a function of the degree of partial melting using the partition coefficients and melting parameters given in Table 5 and plot-

Table 5a. Solid/fluid partition coefficients used in models.

Ds/f	U	Th	Pa	Ra
Discrete fluid addition	0.4	0.9	0.9	0.0010
Continuous flux melting	0.024	0.14	0.05	0.0010
Continuous dehydration	0.4	5	5	0.0012

Coefficients used in the continuous flux melting model are calculated using cpx/fluid partition coefficients for a 5-M (Na, K)Cl fluid from Keppler (1996) and assuming that the slab is an eclogite composed of 50% garnet and 50% cpx. Coefficients used in the continuous dehydration model are calculated using mineral/fluid partition coefficients for a 0.5-M NaCl fluid from Brenan et al. (1995), phengite/fluid partition coefficients for Ba from Zack et al. (2001) and assuming that the slab is composed of 50% garnet, 49.8% cpx and 0.2% phengite. Coefficients for Ra are estimated from Ba partition coefficients using the model of Blundy and Wood (1994).

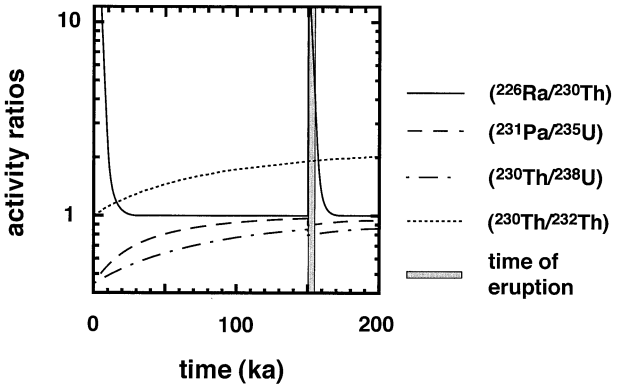

Fig. 10. Evolution of activity ratios in the mantle wedge with time, in the case of a two-step fluid addition, following the model of Turner et al. (2000). Curves are shown for (^{230}Th/^{232}Th) (dotted curve), (^{230}Th/^{238}U) (dotted-dashed curve), (^{231}Pa/^{235}U) (dashed curve) and (^{226}Ra/^{230}Th) ratios (plain curve). A first fluid is added (t = 0), containing U and ^{226}Ra. After 150 ka, a second fluid is added, containing ^{226}Ra and some U. Production and eruption of the magmas is assumed to occur shortly after the second fluid addition (shaded area), to preserve ^{226}Ra excess equal or higher than the (^{226}Ra/^{230}Th) in the HMB end-member (taken to be equal to 3). See text for parameters used.

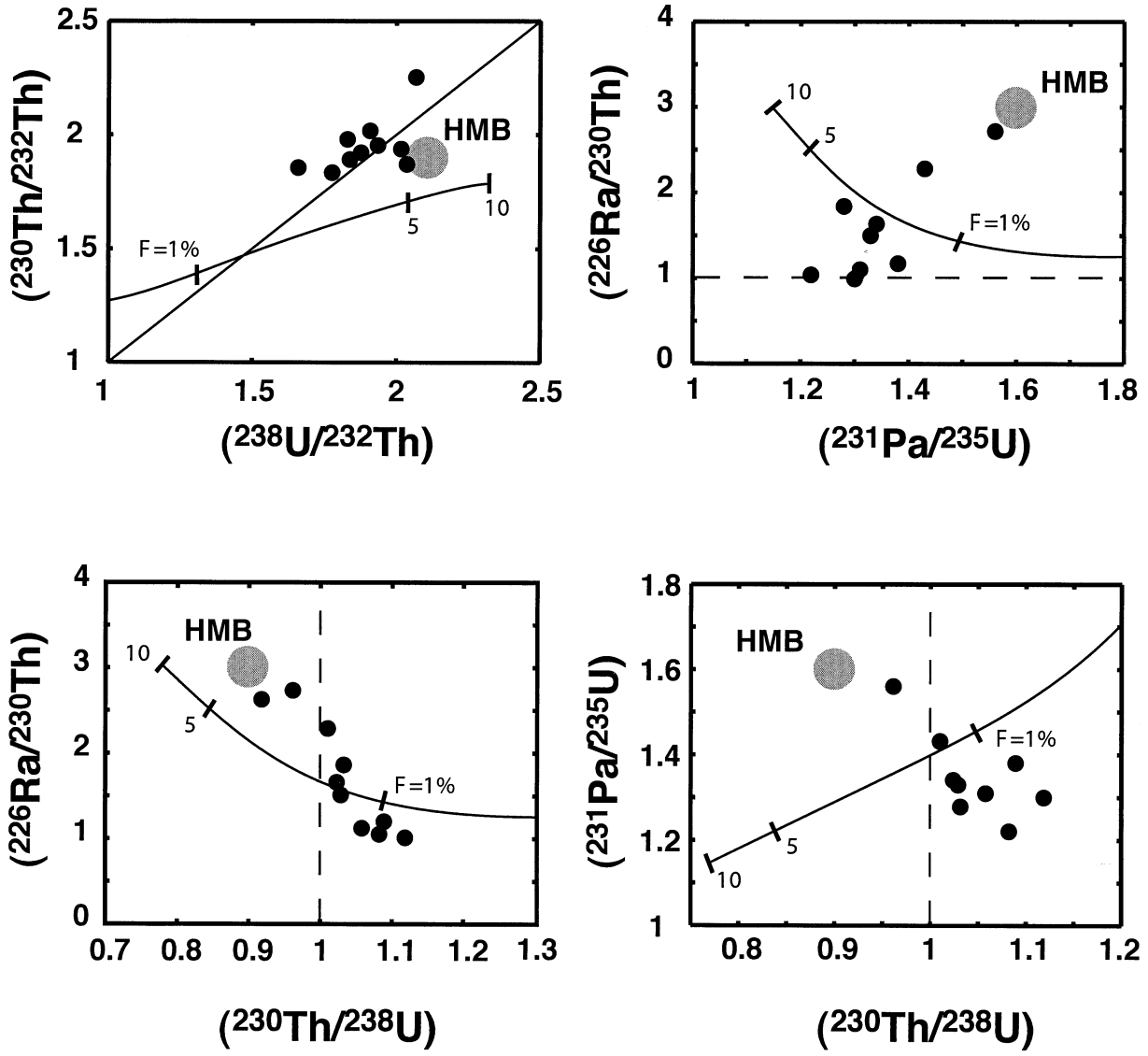

Fig. 11. Model curves for continuous flux melting. Curves represent accumulated magma composition for U-series, as a function of the degree of melting (tick marks). The process ends at *F=10%* and the fraction of fluid extracted from the slab is 3%. See text for model description and other parameters used. It is difficult to reproduce a (^{231}Pa/^{235}U) ratio as high as those of HMB end-member. As U, Th, Pa and Ra are all very incompatible elements, their fractionation is initially controlled by the melting process. Their budget becomes rapidly dominated by the fluid added from the slab and (^{231}Pa/^{235}U) is lowered with time as continuous flux melting proceeds. Diagonal plain line in the upper-left corner diagram and dashed lines in the other diagrams are equilines.

ted on Figure 11. We checked numerically that the size of time steps is sufficiently small such that the process can be considered as continuous (~1000 a). The end of the curves shown on Figure 11 correspond to a final degree of partial melting equal to 10% and a fluid fraction extracted from the slab of 3%. Duration for dehydration is taken to be 1.5 Ma. These calculations show that ^{238}U-^{230}Th-^{226}Ra disequilibrium can be reproduced for the HMB end-member but the model fails to produce significant ^{231}Pa-excesses. Additionally, as U, Th, Pa and Ra are very incompatible elements, melting-induced fractionation will be larger at the inception of the process and decrease with time, as the fluid signature becomes more pronounced. Note that, in this calculation, to maximize the ^{231}Pa excess in the melt, Pa is taken to be slightly mobile in fluid (see Table 5a). If it had been assumed to be immobile, as is commonly thought, the resulting (^{231}Pa/^{235}U) ratios in the accumulated melt would be even lower. One solution for reaching (^{231}Pa/^{235}U) of ~1.6 is to take Pa as mobile as U, but this is very unlikely. Alternatively, the observed (^{231}Pa/^{235}U) activity ratio can be reached by increasing the duration of the continuous flux melting process, for instance, by considering that the duration of dehydration is 5 Ma. However, assuming a subduction rate of 10 cm/yr, this would mean that the dehydration process would take place over a range of depths of 500 km.

As a consequence, this model is rather inefficient to reproduce all U-series characteristic for Kamchatka lavas as it re-

Table 5b. Solid/melt partition coefficients and melting parameters used in models.

Ds/f	U	Th	Pa	Ra	ϕ (‰)	*F* (%)
Continuous flux melting	0.0026	0.0014	1.3×10^{-4}	10^{-5}	1.5	10
Continuous dehydration	0.0026	0.0014	1.3×10^{-4}	10^{-5}	1.5	10
Equilibrium transport melting						
Global	0.0023	0.0023	1.15×10^{-4}	10^{-5}	1.5	10
Garnet lherzolite	0.0025	0.0020	1.3×10^{-4}	10^{-5}		
Spinel lherzolite	0.0020	0.0025	1.0×10^{-4}	10^{-5}		
Dynamic melting	0.0023	0.0023	1.15×10^{-4}	10^{-5}	1.5	10

ϕ and *F* are, respectively, the matrix porosity and final degree of partial melting. Garnet and spinel lherzolite are assumed to have 12% garnet, 8% cpx, and 12% cpx, respectively. Mineral/melt partition coefficients are taken from LaTourrette et al. (1993) and Lundstrom et al. (1994), except for Pa in the case of equilibrium transport and dynamic melting where coefficients are chosen to reproduce the (^{231}Pa/^{235}U) ratio of the HMB end-member.

quires unrealistic ranges of depth for slab dehydration to occur, or Pa to be as fluid-mobile as U.

7.3. Continuous Dehydration

Rather than considering that the mantle wedge is hot enough to melt during slab dehydration, we have considered that fluids accumulate in the peridotite before it reaches its solidus temperature, as proposed for example by Tatsumi (1989). In this model, we assume that melting occurs at the end of the continuous dehydration process. The source of magmas is represented by a box of mantle wedge moving downward, parallel to the slab (Fig. 9c). To a first approximation, slab and mantle wedge are assumed to be perfectly coupled. Fluid is continuously extracted from the slab and transferred to the mantle box. The amount of fluid is assumed to decrease as a function of time following this equation:

$$F = F_{\max} \cdot (1 - e^{-t/\tau}) \tag{1}$$

where τ is a relaxation time corresponding to the time scale over which dehydration occurs, and $F_{\max}$ is the maximum fraction of fluid released. To a first approximation, $F_{\max}$ is taken as the water content of the subducting altered oceanic crust (~3% in Hart and Staudigel, 1989). Calculations were conducted until 90% of the total amount of fluid available has been extracted. The duration of dehydration is determined by the relaxation time scale, and the amount of fluid to be extracted.

Compositions in the metasomatized mantle are calculated as a function of time. Nuclide abundances vary as a function of radioactive decay and production from a parent nuclide, and the amount of nuclide added by the fluid. They are calculated using the following equations:

$$\frac{d^{238}U_{wedge}}{dt} = -\lambda_{238_U} \cdot {}^{238}\mathrm{U}_{wedge} + \frac{d^{238}U_{fluid}}{dt} \tag{2}$$

$$\frac{d^{232}Th_{wedge}}{dt} = -\lambda_{232_{Th}} \cdot {}^{232}Th_{wedge} + \frac{d^{232}Th_{fluid}}{dt} \tag{3}$$

$$\frac{d^{230}Th_{wedge}}{dt} = -\lambda_{230_{Th}} \cdot {}^{230}Th_{wedge} + \lambda_{238_U} \cdot {}^{238}U_{wedge} + \frac{d^{230}Th_{fluid}}{dt} \tag{4}$$

$$\frac{d^{226}Ra_{wedge}}{dt} = -\lambda_{226_{Ra}} \cdot {}^{226}Ra_{wedge} + \lambda_{230_{Th}} \cdot {}^{230}Th_{wedge} + \frac{d^{226}Ra_{fluid}}{dt} \tag{5}$$

where the abundance of a nuclide in the fluid (e.g., for radium, $^{226}\mathrm{Ra}_{\mathrm{fluid}}$), is assumed to follow a Rayleigh distillation law:

$$\frac{d\ln^{226}Ra_{fluid}}{d\ln(1-F)} = \frac{1-D_{Ra}}{D_{Ra}}. \tag{6}$$

D_{Ra} is the solid/fluid partition coefficient for radium. Equations 2 to 6 were solved numerically using the Matlab software.

The composition of the metasomatized mantle is then used to calculate the composition of derived melts, assuming that they are produced by 10% of simple batch melting. Solid/melt partition coefficients used are similar to those used in the previous section (see Table 5b).

If we use the partition coefficients for fluid dehydration estimated in the previous section, based on experimental determination from Keppler (1996), we cannot reproduce the HMB end-member as the model yields large Th-U fractionation (Fig. 12a). Solid/fluid partition coefficients and relaxation time for dehydration have then been chosen to fit the HMB end-member compositions. The relaxation time is 2 Ma, and solid/fluid partition coefficients are given in Table 5a. The corresponding melt compositions are reported on Figure 12. Similar partition coefficients can be calculated, based on experimental determinations, considering mineral/fluid partition coefficients for a 0.5-M NaCl fluid from Brenan et al. (1995) and phengite/fluid partition coefficients for Ba from Zack et al. (2001). In this calculation, the following mineral modes are assumed for the dehydrating slab: garnet: 50, cpx: 49.8 phengite: 0.2. Coefficients for Ra are estimated from Ba coefficients, using the model of Blundy and Wood (1994). In this version of the model, the hydrous phase holds on to Ra more efficiently than a dry eclogite. In the case of a dry eclogite, radium is stripped from the slab and no ^{226}Ra excess is produced once the target value for (^{230}Th/^{232}Th) is reached (~1.9).

Following this model, the HMB end-member compositions would be reached after 410 ka of continuous fluid addition. The model yields, at 410 ka, (^{230}Th/^{232}Th) = 1.9, (^{230}Th/^{238}U) = 0.89, (^{231}Pa/^{235}U) = 1 and (^{226}Ra/^{230}Th) = 5.9. An important conclusion is that, in the context of continuous fluid addition, the time scale of dehydration has to be relatively long to

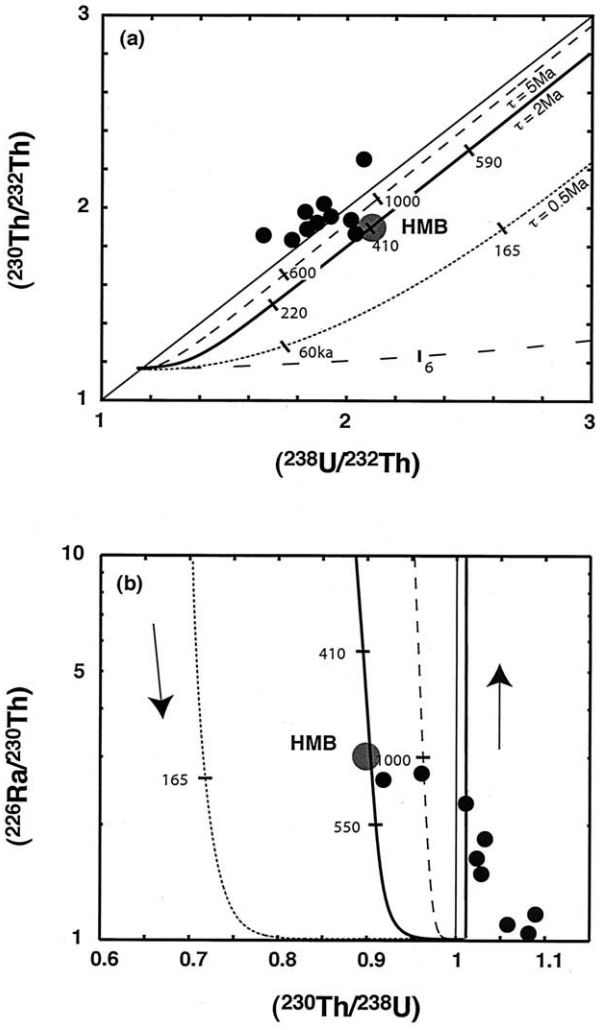

Fig. 12. Model curves for continuous dehydration followed by batch melting. (a) ^{230}Th-^{238}U isochron diagram, (b) (^{226}Ra/^{230}Th) plotted against (^{230}Th/^{238}U) ratios. Curves show time evolution of activity ratios in the melts produced by 10% melting of the metasomatized mantle. Labels on the curves are dehydration duration before melting, for a given relaxation time. See text for model description and parameters used. Long-dashed curve show compositions using mineral/fluid partition coefficients from Keppler (1996) and for a dehydration relaxation time of 2 Ma. Dotted, thick and dashed curves are compositions calculated using mineral/fluid partition coefficients from Brenan et al. (1995) and for dehydration relaxation time equal to 0.5, 2 and 5 Ma, respectively. Black dots are Kamchatka data. Arrows show the evolution of activity ratios with time. U-series values for HMB end-member are reached for a dehydration relaxation time of 2 Ma and dehydration duration of 410 ka. These results are obtained using solid/fluid partition coefficients from Brenan et al. (1995), phengite/fluid partition coefficients from Zack et al. (2001) and assuming that the slab is a phengite-bearing eclogite with 0.2% phengite. Coefficients for Ra are estimated from coefficients for Ba using the model of Blundy and Wood (1994). Solid/fluid partition coefficients from Keppler (1996) do not match the CKD data. Plain lines are equilines for the ^{230}Th-^{238}U system.

produce the high (^{230}Th/^{232}Th) found in CKD lavas (in this case, $\tau = 2$ *Ma*). For significantly shorter time scales, when (^{230}Th/^{232}Th) is reached, ^{226}Ra excess is lower than required (τ = 0.5 Ma; Fig. 12).

Alternatively, it is possible that the mantle wedge is not perfectly coupled to the slab and is dragged down more slowly (Turner and Hawkesworth, 1997). In this case, for a slab/mantle velocity ratio >1 and τ = 2 Ma, the model yields ^{238}U excesses too large compared to those observed (not shown). For instance, for slab/mantle velocity ratio = 2 and τ = 2 Ma, the target (^{230}Th/^{232}Th) ratio (~1.9) is reached after 250 ka and (^{230}Th/^{238}U) is then equal to 0.80, which is low compared to the value for the HMB end-member (0.90). To reproduce the observed HMB compositions, a larger time scale must be considered but it implies that dehydration of the slab occurs over an unrealistic range of depths. In a case where slab/mantle velocity ratio would be 2 and slab velocity 10 cm/yr, the time scale that fits the HMB compositions is 4 Ma. This implies that dehydration would occur over a range of depths of 400 km.

The ^{231}Pa-^{235}U disequilibrium is not discussed here, as the model is unable to produce significant ^{231}Pa excess. This results mostly from using a simple batch melting model, which offers little leverage to counterweight the U-series fractionation due to fluid addition. In the next section, some melting models are reviewed to explain (^{231}Pa/^{235}U) ratios >1.

To summarize, continuous dehydration seems a possible model for explaining ^{238}U-^{230}Th-^{226}Ra signature in the HMB end-member. The dehydrating slab is assumed to have a phengite eclogite composition with 0.2% hydrous phase. The time scale for dehydration is taken to be 2 Ma and the preferred model assumed that the mantle wedge is perfectly coupled to the slab. Even if it is not clear that continuous dehydration can account for U-Th-Ra characteristics in other arcs, it seems that, in the case of Kamchatka, both discrete and continuous fluid addition can explain ^{238}U-^{230}Th-^{226}Ra characteristics in the HMB end-member.

7.4. Melting Models for Kamchatka Magmas Genesis

A previous study of the Tonga-Kermadec arc has proposed melting by equilibrium transport to explain observed (^{231}Pa/^{235}U) ratios >1 in the Kermadec lavas (Bourdon et al., 1999b). This model is tested here for the Kamchatka data using the whole U-series data set. Similarly, dynamic melting is also evaluated. In each model, the mantle wedge source is assumed to display initial ^{226}Ra excess, moderate ^{238}U excess and ^{231}Pa-^{235}U close to secular equilibrium, as suggested in the previous section.

7.4.1. Equilibrium transport melting

In this section, we have attempted to reproduce the (^{231}Pa/^{235}U) ratio observed in the HMB end-member with the equilibrium transport model developed by Spiegelman and Elliott (1993). This model implies that upwelling occurs within the mantle wedge. This may be relevant in the case of the Central Kamchatka Depression, as it is a zone of rifting, therefore possibly associated with upwelling in the underlying mantle. Further evidence for upwelling comes from the study of Levin et al. (2002) who have suggested a possible mantle upwelling below CKD, probably linked to a recent slab loss.

As seen in section 6.1, ^{226}Ra excesses are thought to be generated by fluid addition. To preserve the fluid-derived ^{226}Ra excesses, the residence time of radium in the melting column must be short relative to its half-life (1600 a). This is only

possible if the melting rate and the corresponding solid upwelling velocity are large enough to have the ^{226}Ra rapidly stripped to the melt. The melting column is assumed to range from 10 to 30 kbar with transition between garnet and spinel lherzolites at 20 kbar. Other melting parameters can be found in Table 5b. It is shown on Figure 13 that the HMB end-member composition can be roughly matched, taking the upwelling velocity to be equal to 13 cm/yr and assuming the following initial activity ratios in the source: (^{230}Th/^{238}U) = 0.8, (^{231}Pa/^{235}U) = 0.9 and (^{226}Ra/^{230}Th) = 4. These values correspond to activity ratios in the wedge, calculated after either discrete or continuous fluid addition as shown in sections 7.1 and 7.3.

Consequently, melting by equilibrium porous flow seems a viable mechanism for explaining Kamchatka data as long as a fluid addition takes place before melting. However, most of ^{226}Ra-^{230}Th fractionation is controlled by the matrix porosity and the final (^{226}Ra/^{230}Th) value is derived mostly from melting except for very large upwelling velocity (1 m/yr). Therefore, it is unclear how this model can produce the correlations between ^{226}Ra/^{230}Th and trace element ratios indicative of fluid addition (Sr/Th or Rb/Th). Consequently, we have considered an alternative model involving rapid extraction of the magmas, allowing preservation of slab-derived ^{226}Ra excess without the requirement of large upwelling velocity.

7.4.2. Dynamic melting

In this model, melt is produced in equilibrium with the matrix and at once extracted into channels where it travels to the surface at infinite velocity. The matrix porosity is kept constant during the whole melting process (McKenzie, 1985). Hence, there is no need for an upwelling melting column as the matrix can be taken to migrate upward or downward (parallel to the slab) as magmas are extracted from all levels of the source. In the latter case, dynamic melting is similar to the continuous flux melting model (section 7.2) with the difference that fluid addition occurs only before the melting process and not during it.

Using similar partition coefficients and initial conditions to the equilibrium transport model, we have attempted to reproduce HMB end-member compositions. Porosity and solid/melt partition coefficients are similar to those used in the equilibrium transport model (Table 5b). The results of our calculation are shown on Figure 14, where the curves correspond to variable degrees of melting. The HMB end-member compositions can be reproduced after 10% of partial melting, taking the melting rate to be equal to 1.3×10^{-4} kg/m^3/yr. Thus, if we assume fluid addition to the mantle wedge source before melting, it is possible to reproduce the compositions of the HMB end-member using a dynamic melting model. This model is preferred to equilibrium transport melting, as in this case, there is no need to invoke excessively high upwelling velocity within the mantle wedge.

To summarize, continuous dehydration and two-step fluid addition are two possible models for describing mantle metasomatism under the Central Kamchatka Depression. It has been shown that equilibrium transport model is a plausible model for describing mantle melting beneath arcs, but requires very high upwelling rates in the wedge. We prefer a dynamic melting model as it yields similar results without the necessity of extreme values for melting parameters. These models allow us to reproduce compositions for HMB end-member. In the next section, various hypothesis are investigated for explaining the HAA end-member characteristics.

8. SLAB MELTING UNDER THE CENTRAL KAMCHATKA DEPRESSION

The HAA end-member is characterized by (^{230}Th/^{238}U) and (^{231}Pa/^{235}U) greater than unity and ^{226}Ra-^{230}Th in secular equilibrium. Interestingly, it also displays more radiogenic ^{187}Os/^{188}Os ratios and higher La/Yb ratios than the HMB endmember, but similar Nd, Sr and Pb isotope compositions.

There are a priori three possible explanations for these characteristics: (1) addition of sediments to the wedge, (2) crustal assimilation or (3) addition of a slab melt. Out of these three possibilities, sediment addition can be directly ruled out as ^{207}Pb/^{206}Pb and ^{143}Nd/^{144}Nd ratios in both HMB and HAA show nearly constant MORB-like values. Sediment addition is thus unlikely to explain HAA end-member compositions as it would increase ^{207}Pb/^{206}Pb and decrease ^{143}Nd/^{144}Nd ratios.

Crustal assimilation is expected to display similar characteristics to those observed in the HAA end-member because the crust of the Kamchatka arc is thought to be mafic and should yield similar Pb and Nd isotope ratios. However, to produce (^{230}Th/^{238}U) >1, garnet needs to be a residual phase as Kamchatka crust melts, and this implies that crustal assimilation must occur at pressure >10 kbar. As the overriding crust is only 30 km thick, it is hard to argue for the presence of garnet during crustal assimilation since garnet is not stable below $\sim$14 kbar in mafic compositions. Note that while crustal assimilation has already been invoked for explaining ^{230}Th-excess in Chile arc magmas (Bourdon et al., 2000), in this case, the overriding crust was 70 km thick, which allowed garnet to be a residual phase during crustal melting.

It has been suggested that melting on the edge of the subducted oceanic crust may account for chemical characteristics of Sheveluch lavas, in the northernmost part of the Central Kamchatka Depression (Yogodzinski et al., 2001). Recent seismic evidence has shown that there could have been a slab loss 2 Ma ago beneath the CKD (Levin et al., 2002). This event must have increased the slab edge temperature so as to induce slab melting. We now show that the distinctive signature of the HAA lavas could in fact reflect a mixture between a slab melt and melts from a hydrous mantle.

Firstly, Mg# for high-alumina basalts and andesites range from 0.41 to 0.87 with 40% of the lavas exhibiting values >0.6, which implies that they can be considered as primitive. The ^{230}Th excesses high La/Yb and ^{187}Os/^{188}Os ratios are found in lavas with molar Mg# >0.6. It is thus unlikely that these characteristics are derived from a shallow process linked to fractional crystallization, such as crustal assimilation. Secondly, expected ^{187}Os/^{188}Os ratios in the subducted oceanic crust were estimated based on the composition of zero-age Pacific oceanic crust (Schiano et al., 1997). We have assumed that the ^{187}Re-^{187}Os system evolves as a closed system for 80 Ma (age of the subducted oceanic crust). The estimated ^{187}Os/^{188}Os (1.84) is much higher than the ratios found in the HAA end-member and could well account for the more radiogenic composition of the HAA. Thirdly, the HAA end-member has

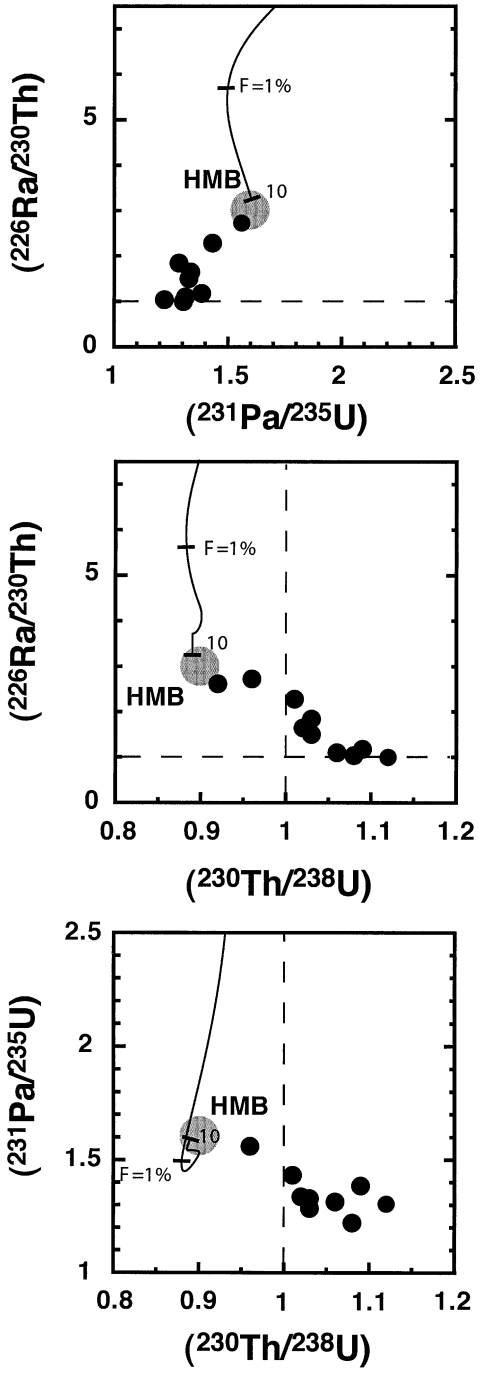

Fig. 13. Parent/daughter activity ratios in magmas produced by equilibrium transport melting. Calculations were done using UserCalc v2.0 (Spiegelman, 2000). The curves show the evolution of activity ratios in the magma as a function of the degree of partial melting, *F*. Final degree of partial melting is 10%. Tick marks are for $F = 1$ and 10%. See text and Table 5b for parameters used. Before melting, the source is assumed to have $(^{230}Th/^{238}U) = 0.8$, $(^{231}Pa/^{235}U) = 0.9$ and $(^{226}Ra/^{230}Th) = 4$, as a consequence of fluid addition to the wedge by discrete or continuous dehydration of the slab. For 10% of melting, activity ratios in HMB end-member can be matched. The main problem with this model is that, unless considering very large upwelling velocities, fluid-derived ^{226}Ra excesses are totally overprinted by excesses produced during melting. This is unlikely to be the case for Kamchatka as ^{226}Ra excess is correlated with indices of a fluid component such as high Ba/Th, Rb/Th and Sr/Th ratios. Dashed lines are equilines.

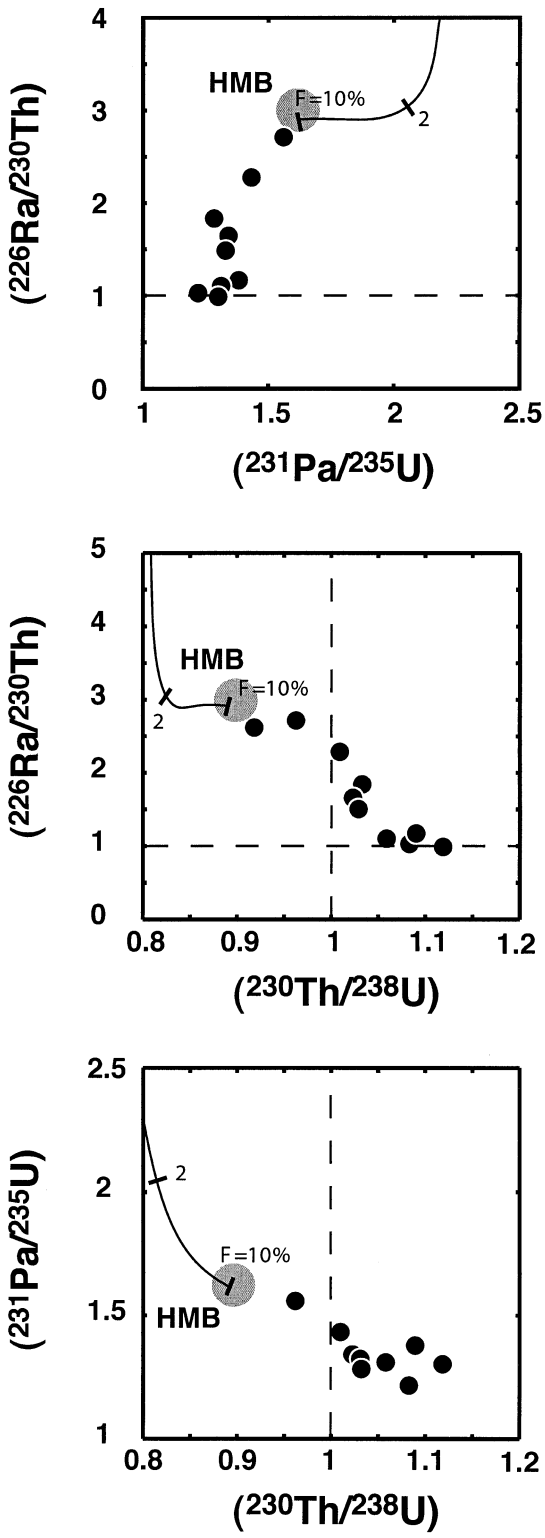

Fig. 14. Model curves for daughter/parent activity ratios in magmas produced by dynamic melting. The curves show the evolution of magma composition as a function of the degree of partial melting (tick marks). Similarly to the equilibrium transport melting model on Figure 13, the source is assumed to have $(^{230}Th/^{238}U)$ and $(^{231}Pa/^{235}U) < 1$, and $(^{226}Ra/^{230}Th) > 1$, before melting. See text and Table 5b for parameters used. Suitable activity ratios for HMB end-member are reached after 10% of melting. Dashed lines are equilines.

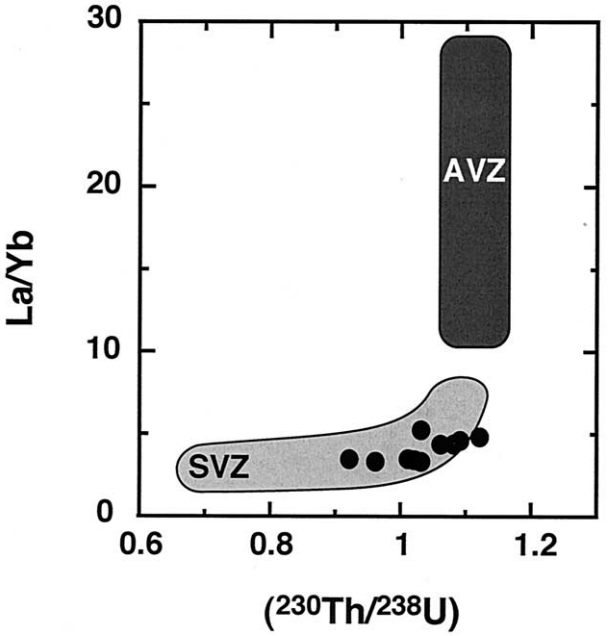

Fig. 15. La/Yb ratios vs. (^{230}Th/^{238}U) activity ratios diagram. SVZ and AVZ fields represent, respectively, data for the Southern and Austral volcanic zones from South Chile (Sigmarsson et al., 1998). ^{230}Th excess for AVZ lavas has been explained by melting of the subducted oceanic crust. Kamchatka data (black dots) are located in an intermediate field and lavas may represent mixtures of hydrous mantle melt with slab-derived melts (see text for discussion).

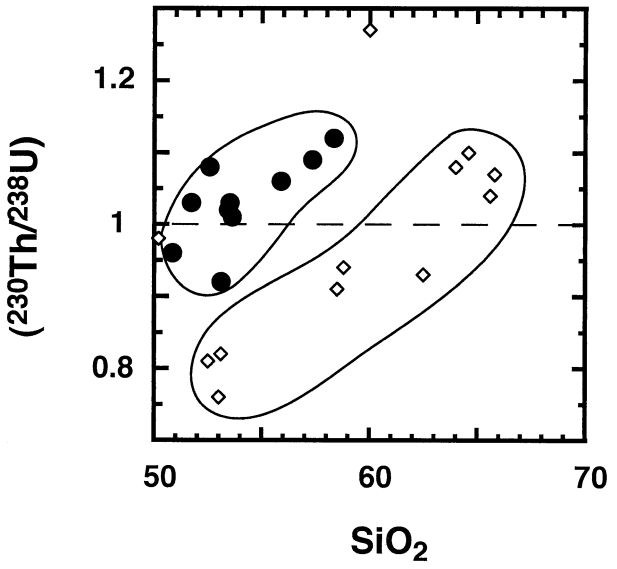

Fig. 16. (^{230}Th/^{238}U) activity ratios vs. SiO_2 content (wt.%). Kamchatka data (black dots) are compared with data from South Chile (diamonds; Sigmarsson et al., 1998). They show similar trends, where ^{230}Th excess are found in high-silica rocks and low-silica magmas are characterized by ^{238}U excess. For both regions, this may reflect mixing between low-silica magma produced by melting of the hydrated mantle wedge, and high-silica magmas derived from melting of the subducted oceanic crust. These two processes may account for the origin of HMB and HAA end-members, respectively.

typical signature for melting in the presence of garnet (^{230}Th excess and high La/Yb). Similar signatures were found for the adakites of South Chile (Sigmarsson et al., 2002; Fig. 15). Moreover, in a (^{230}Th/^{238}U) vs. SiO_2 diagram (Fig. 16), South Chile and Kamchatka magmas show similar positive trends. This can be interpreted as a mixing between low-silica hydrated mantle melts with ^{238}U excess and high-silica oceanic crust melts with ^{230}Th excess. This observation could possibly account for the origin of HMB and HAA, respectively.

Furthermore, in a (^{226}Ra/^{230}Th) vs. (^{230}Th/^{238}U) diagram (Fig. 17), South Chile and Kamchatka lavas also exhibit similar negative trends. The HAA end-member, with ^{230}Th excess over ^{238}U and ^{226}Ra-^{230}Th in secular equilibrium, may be derived from slab melting in the presence of residual garnet and phengite. Indeed, melting in presence of residual garnet accounts for (^{230}Th/^{238}U) >1, whereas residual phengite may explain the absence of ^{226}Ra-^{230}Th disequilibrium, as Ba (Ra) is more compatible in this mineral than Th.

Finally, the presence of residual rutile during slab melting could also account for lower ^{231}Pa excess over ^{235}U, in HAA end-member, as rutile is believed to retain HFSE, and so, probably Pa (rutile/melt partition coefficients for Nb and Ta range from 100–500; Foley et al., 2000). Based on the model of Blundy and Wood (1994), the estimated D_{Pa} in rutile is $\sim$0.5. It is not impossible that residual rutile is present in the subducted oceanic crust as Klemme et al. (2002) have recently suggested that this phase may be stable until 3 GPa.

It is thus likely that HAA end-member characteristics indicate the involvement of slab-derived melt in the source. The U-series characteristics that we have inferred for slab melt should be looked for at other arc settings where the presence of slab melts has been inferred.

9. CONCLUSIONS

The relationships between parent/daughter activity ratios of ^{226}Ra-^{230}Th-^{238}U and ^{231}Pa-^{235}U systems have been interpreted as the result of mixing between high-magnesia basalt (HMB) and high-alumina andesite (HAA) end-members exhibiting distinct U-series signatures.

Several scenarii including combinations of dehydration and melting are explored for explaining the origin of HMB and HAA. The HMB end-member is explained by melting of metasomatized mantle following slab dehydration. It turns out that continuous dehydration may be a suitable model for describing slab dehydration as long as melting occurs at the end of the process and not during it. Another possibility is that dehydration occurs as a two step fluid addition. In this case, the first fluid addition must have occurred 150 ka ago whereas the second takes place less than a few thousand years before eruption. The inferred composition of the slab for these models is a phengite-bearing eclogite.

The melting model that best fits U-series data for the HMB end-member is a dynamic melting model where melt is rapidly extracted from the melting region. Melting with equilibrium transport could also be a relevant model but it implies extreme values for upwelling velocity in the wedge.

Finally, the high-alumina andesite end-member compositions can be explained by melting of the oceanic crust, as shown by their high La/Yb ratios and ^{230}Th excesses associated with Mg# >0.6. U-series characteristics for HAA end-member

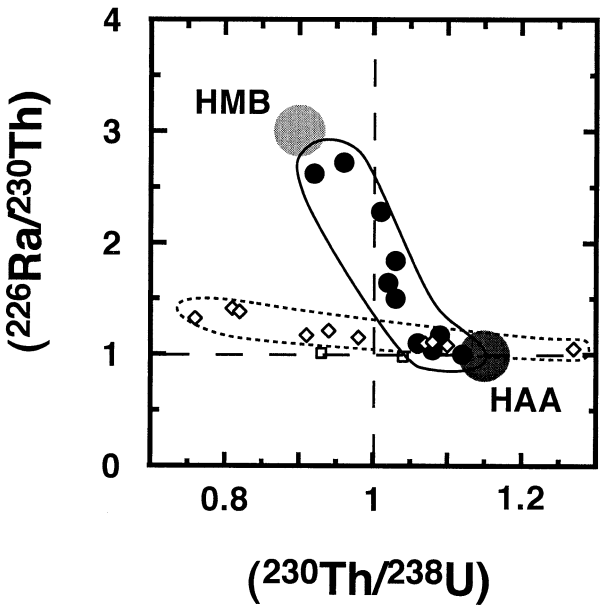

Fig. 17. ($^{226}Ra/^{230}Th$) vs. ($^{230}Th/^{238}U$) for Kamchatka (black dots) and South Chile lavas (diamonds and squares; Sigmarsson et al., 2002). Both regions show similar trends where ^{238}U and ^{226}Ra excesses are associated (HMB end-member), and lavas with ^{230}Th excess are characterized by ^{226}Ra-^{230}Th in secular equilibrium (HAA end-member). Characteristics for HMB are explained by melting of a hydrated mantle, enriched in U and Ra relative to Th, before melting; whereas those for HAA can be understood by mixing with subducted slab melts in the presence of residual garnet and phengite (see text for details). Residual garnet yields ^{230}Th excess while phengite, as it is expected to retain radium and barium during melting, leads to reduced or absent ^{226}Ra-^{230}Th disequilibrium. Dashed lines are equilines.

suggest that the melting oceanic crust is a phengite-bearing eclogite with residual rutile, which should retain Ra and Pa more efficiently than other slab mineralogies. This is consistent with the composition inferred from dehydration models.

High-magnesia basalts and high-alumina andesites are not directly genetically linked, rather they represent two magma types that may be present at other arcs.

Acknowledgments— Craig Lundstrom, Simon Turner and Tim Elliott are thanked for their detailed and constructive reviews, which contributed to a large improvement of the manuscript. We would like to thank the Associate Editor, Alan Brandon for his patience and helpful comments. Gerhard Wörner and Tatiana Churikova are thanked for very helpful discussions. We thank Kevin Burton for the access to the ICP-MS at the Open University. We would also like to thank M. Semet for providing samples and trace element data. We also thank M. Moreira and C. J. Allègre for helpful remarks on an earlier version of the manuscript.

Associate editor: A. Brandon

REFERENCES

Allègre C. J. and Condomines M. (1982) Basalt genesis and mantle structure studied through Th-isotopic geochemistry. *Nature* **299,** 21–24.

Alves S., Schiano P., Capmas F., and Allègre C. J. (2002) Osmium isotope binary mixing arrays in arc volcanism. *Earth Planet. Sci. Lett.* **198,** 355–369.

Basaltic Volcanism Study Project (1981) *Basaltic Volcanism on the Terrestrial Planets*. Pergamon, New York.

Blundy J. and Wood B. (1994) Prediction of crystal-melt partition coefficients from elastic moduli. *Nature* **372,** *6505,* 452–454.

Bohlen S. R., Boettcher A. L., and Clements J. D. (1983) Stability of phlogopite-quartz and sanidine-quartz: A model for melting in the lower crust. *Contrib. Mineral. Petrol.* **83,** 270–277.

Bourdon B., Zindler A., Elliott T., and Langmuir C. H. (1996) Constraints on mantle melting at mid-ocean ridges from global ^{238}U-^{230}Th disequilibrium data. *Nature* **384,** 231–235.

Bourdon B., Joron J. L., and Allègre C. J. (1999a) A method for ^{231}Pa analysis by thermal ionization mass spectrometry in silicate rocks. *Chem. Geol.* **157,** 147–151.

Bourdon B., Turner S., and Allègre C. J. (1999b) Melting dynamics beneath the Tonga-Kermadec island arc inferred from ^{231}Pa-^{235}U systematics. *Science* **286,** 2491–2493.

Bourdon B., Wörner G., and Zindler A. (2000) U-series evidence for crustal involvement and magma residence times in the petrogenesis of Parinacota volcano, Chile. *Contrib. Mineral. Petrol.* **139,** 458–469.

Bourdon B., Turner S., and Dosseto A. (submitted) Dehydration and partial melting in subduction zones: Constraints from U-series disequilibria, in press. J. Geophys. Res.

Brenan J. M., Shaw H. F., Ryerson F. J., and Phinney D. L. (1995) Mineral-aqueous fluid partitioning of trace elements at 900°C and 2.0 GPa: Constraints on the trace element chemistry of mantle and deep crustal fluids. *Geochim. Cosmochim. Acta* **59,** 3331–3350.

Chabaux F. (1993) *Systématique ^{238}U-^{230}Th-^{226}Ra Dans les Roches Volcaniques: Développements Analytiques et Etude des Processus de Fusion*. Ph.D. dissertation, Université Paris 7.

Chabaux F., Hémond C., and Allègre C. J. (1999) ^{238}U-^{230}Th-^{226}Ra disequilibria in the Lesser Antilles arc: Implications for mantle metasomatism. *Chem. Geol.* **153,** 171–185.

Cheng H., Edwards R. L., Hoff J., Gallup C. D., Richards D. A., and Asmerom Y. (2000) The half-lives of uranium-234 and thorium-230. *Chem. Geol.* **169,** *1–2,* 17–33.

Clark S. K., Reagan M. K., and Plank T. (1998) Trace element and U-series systematics for 1963-1965 tephras from Irazu volcano, Costa Rica: Implications for magma generation processes and transit times. *Geochim. Cosmochim. Acta* **62,** 2689–2699.

Claude-Ivanaj C. (1997) *Systématique ^{238}U-^{230}Th-^{226}Ra Appliquée au Volcanisme Actif Océanique: Contraintes sur la Durée et les Processus de Formation des Magmas*. Ph.D. dissertation, Université Paris 7.

Claude-Ivanaj C., Bourdon B., and Allègre C. J. (1998) Ra-Th-Sr isotope systematics in Grande Comore Island: A case study of plume-lithosphere interaction. *Earth Planet. Sci. Lett.* **164,** 99–117.

Delany J. M. and Helgeson H. C. (1978) Calculation of the thermodynamic consequences of dehydration in subducting oceanic crust to 100 kb and >800 °C. *Am. J. Sci.* **278,** 638–686.

DeMets C. R., Gordon G., Argus D. F., and Stein S. (1990) Current plate motions. *Geophys. J. Int.* **101,** 425–478.

Elliott T., Plank T., Zindler A., White W., and Bourdon B. (1997) Element transport from subducted slab to juvenile crust at the Mariana arc. *J. Geophys. Res.* **102,** 14991–15019.

Foley S. F., Barth M. G., and Jenner G. A. (2000) Rutile/melt partition coefficients for trace elements and an assessment of the influence of rutile on the trace element characteristics of subduction zone magmas. *Geochim. Cosmochim. Acta* **64,** 933–938.

Gill J. (1981) *Orogenic Andesites and Plate Tectonics*. Springer-Verlag, Berlin, Germany.

Gill J. B. and Williams R. W. (1990) Th isotopes and U-series studies of subduction-related volcanic rocks. *Geochim. Cosmochim. Acta* **54,** 1427–1442.

Gorbatov A., Kostoglodov V., Gerardo S., and Gordeev E. (1997) Seismicity and structure of the Kamchatka subduction zone. *J. Geophys. Res.* **102,** 17883–17898.

Green D. H. (1973) Contrasted melting relations in a pyrolite upper mantle under mid-ocean ridge, stable crust and island arc environments. *Tectonophysics* **17,** 285–297.

Hart S. R. and Staudigel H. (1989) Isotopic characterization and identification of recycled components. In *Crustal/Mantle Recycling at Convergence Zones* (eds. S. R. Hart and L. Gülen), pp. 15–28. Kluwer Academic, Amsterdam, the Netherlands.

Hawkesworth C. J., Turner S. P., McDermott F., Peate D. W., and van Calsteren P. (1997) U-Th isotopes in arc magmas: Implications for element transfer from the subducted crust. *Science* **276,** 551–555.

Hochstaedter A. G., Kepezhinskas P., Defant M., Drummond M., and Koloskov A. (1996) Insights into the volcanic arc mantle wedge from magnesian lavas from the Kamchatka arc. *J. Geophys. Res.* **101,** *B1,* 697–712.

Hofmann A. W. (1988) Chemical differentiation of the Earth: The relationship between mantle, continental crust, and oceanic crust. *Earth Planet. Sci. Lett.* **90,** 297–314.

Hoogewerff J. A., van Bergen M. J., Vroon P. Z., Hertogen J., Wordel R., Sneyers A., Nasution A., Varekamp J. C., Moens H. L. E., and Mouchel D. (1997) U-series, Sr-Nd-Pb isotope and trace-element systematics across an active island arc-continent collision zone: Implications for element transfer at the slab-wedge interface. *Geochim. Cosmochim. Acta* **61,** 1057–1072.

Ishikawa T. and Nakamura E. (1994) Origin of the slab component in arc lavas from across-arc variation of B and Pb isotopes. *Nature* **370,** 205–207.

Ishikawa T. and Tera F. (1997) Source, composition and distribution of the fluid in the Kurile mantle wedge: Constraints from across-arc variations of B/Nb and B isotopes. *Earth Planet. Sci. Lett.* **152,** 123–138.

Iwamori H. (1998) Transportation of H_2O and melting in subduction zones. *Earth Planet. Sci. Lett.* **160,** 65–80.

Kepezhinskas P., McDermott F., Defant M. J., Hochstaedter A., Drummond M. S., Hawkesworth C. J., Koloskov A., Maury R. C., and Bellon H. (1997) Trace element and Sr-Nd-Pb isotopic constraints on a three-component model of Kamchatka arc petrogenesis. *Geochim. Cosmochim. Acta* **61,** 577–600.

Keppler H. (1996) Constraints from partitioning experiments on the composition of subduction-zone fluids. *Nature* **380,** 237–240.

Kersting A. B. and Arculus R. J. (1994) Klyuchevskoy volcano, Kamchatka, Russia: The role of high-flux recharged, tapped, and fractionated magma chamber(s) in the genesis of high-Al_2O_3 from high-MgO basalt. *J. Petrol.* **35,** *1,* 1–41.

Klemme S., Blundy J. D., and Wood B. J. (2002) Experimental constraints on major and trace elements partitioning during partial melting of eclogite. *Geochim. Cosmochim. Acta* **66,** 3109–3123.

Kushiro I., Shono Y., and Akimoto S.-I. (1967) Stability of phlogopite at high pressures and possible presence of phlogopite in the Earth's upper mantle. *Earth Planet. Sci. Lett.* **3,** 197–203.

Lambert I. B. and Wyllie P. J. (1972) Melting of gabbro (quartz eclogite) with excess water to 35 kilobars with geological applications. *J. Geol.* **80,** 693–720.

LaTourette T. Z., Kennedy A. K., and Wasserburg G. J. (1993) Thorium-uranium fractionation by garnet; evidence for a deep source and rapid rise of oceanic basalts. *Science* **261,** 739–742.

Levin V., Shapiro N., Park J., and Ritzwoller M. (2002) Seismic evidence for catastrophic slab loss beneath Kamchatka. *Nature* **418,** 763–767.

Lundstrom C. C., Shaw H. F., Ryerson F. J., Phinney D. L., Gill J. B., and Williams Q. (1994) Compositional controls on partitioning of U, Th, Ba, Pb, Sr and Zr between clinopyroxene and haplobasaltic melts: Implications for uranium series disequilibria in basalts. *Earth Planet. Sci. Lett.* **128,** 407–423.

Manhès G. (1981). *Developpement de l'Ensemble Chronomètrique U-Th-Pb: Contribution à la Chronologie Initiale du Système Solaire*. Ph.D. dissertation, Université Paris. 6.

McKenzie D. (1985) ^{230}Th-^{238}U disequilibrium and the melting processes beneath ridge axes. *Earth Planet. Sci. Lett.* **72,** 149–157.

Melekestsev I., Khrenov A. P., and Kozhemyaka N. N. (1991) Tectonic position and general description of volcanoes of Northern group and Sredinny range. In *Active Volcanoes of Kamchatka, Vol. 1, Part II* (ed. A. O. Sciences), pp. 79–97.

Millhollen G. L., Irving A. J., and Wyllie P. J. (1974) Melting interval of peridotite with 5.7 per cent water to 30 kbars. *J. Geol.* **82,** 575–587.

Miyashiro A. (1974) Volcanic rock series in island arcs and active continental margins. *Am. J. Sci.* **274,** 321–355.

Peate D. W., Hawkesworth C. J., van Calsteren P. W., Taylor R. N., and Murton B. J. (2001) ^{238}U-230. Th constraints on mantle upwelling and plume-ridge interaction along the Reykjanes Ridge. *Earth Planet. Sci. Lett.* **187,** 259–272.

Pickett D. A. and Murrell M. T. (1997) Observations of ^{231}Pa/^{235}U disequilibrium in volcanic rocks. *Earth Planet. Sci. Lett.* **148,** 259–271.

Pineau F., Semet M. P., Grassineau N., Okrugin V. M., and Javoy M. (1999) The genesis of the stable isotope (O,H) record in arc magmas: The Kamtchatka's case. *Chem. Geol.* **135,** 93–124.

Rea D. K. (1993) Paleoceanographic record of North Pacific quantified. *Eos: Trans. Am. Geophys. Union* **74,** 406–411.

Reagan M. K. and Gill J. B. (1989) Coexisting calcalkaline and high-niobium basalts from Turrialba volcano, Costa Rica: Implications for residual titanates in arc magma sources. *J. Geophys. Res.* **94,** *B4,* 4619–4633.

Reagan M. K., Morris J. D., Herstrom E. A., and Murrell M. T. (1994) Uranium series and beryllium isotope evidence for an extended history of subduction modification of the mantle below Nicaragua. *Geochim. Cosmochim. Acta* **58,** 4199–4212.

Schiano P., Birck J. L., and Allègre C. J. (1997) Osmium-strontium-neodymium-lead isotopic covariations in mid-ocean ridge basalt glasses and the heterogeneity of the upper mantle. *Earth Planet. Sci. Lett.* **150,** 363–379.

Schmidt M. W. and Poli S. (1998) Experimentally based water budgets for dehydrating slabs and consequences for arc magma generation. *Earth Planet. Sci. Lett.* **163,** 361–379.

Shibata T. and Nakamura E. (1997) Across-arc variations of isotope and trace element compositions from Quaternary basaltic volcanic rocks in northeastern Japan: Implications for interaction between subducted oceanic slab and mantle wedge. *J. Geophys. Res.* **102,** *B4,* 8051–8064.

Sigmarsson O., Condomines M., and Fourcade S. (1992) A detailed Th, Sr and O isotope study of Hekla; differentiation processes in an Icelandic volcano. *Contrib. Mineral. Petrol.* **112,** *1,* 20–34.

Sigmarsson O., Martin H., and Knowles J. (1998) Melting of a subducting oceanic crust from U-Th disequilibria in austral Andean lavas. *Nature* **394,** 566–569.

Sigmarsson O., Chmeleff J., Morris J., and Lopez-Escobar L. (2002) Origin of ^{226}Ra-^{230}Th disequilibria arc lavas from southern Chile and magma transfer time. *Earth Planet. Sci. Lett.* **196,** 189–196.

Spiegelman M. (2000) UserCalc: A web-based uranium series calculator for magma migration problems. *Geochem. Geophys. Geosyst.* **1**.

Spiegelman M. and Elliott T. (1993) Consequences of melt transport for uranium series disequilibrium in young lavas. *Earth Planet. Sci. Lett.* **118,** 1–20.

Tatsumi Y. (1989) Migration of fluid phases and genesis of basalt magmas in subduction zones. *J. Geophys. Res.* **94,** *B4,* 4697–4707.

Tatsumi Y. and Nakamura E. (1986) Composition of aqueous fluid from serpentinite in the subducted lithosphere. *Geochem. J.* **20,** *4,* 191–196.

Turner S. and Hawkesworth C. (1997) Constraints on flux rates and mantle dynamics beneath island arcs from Tonga-Kermadec lava geochemistry. *Nature* **389,** 568–573.

Turner S., Hawkesworth C., van Calsteren P., Heath E., Macdonald R., and Black S. (1996) U-series isotopes and destructive plate margin magma genesis in the Lesser Antilles. *Earth Planet. Sci. Lett.* **142,** 191–207.

Turner S., McDermott F., Hawkesworth C., and Kepezhinskas P. (1998) A U-series study of lavas from Kamchatka and the Aleutians: Constraints on source composition and melting processes. *Contrib. Mineral. Petrol.* **133,** 217–234.

Turner S., Bourdon B., Hawkesworth C., and Evans P. (2000) ^{226}Ra-^{230}Th evidence for multiple dehydration events, rapid melt ascent and time scales of differentiation beneath the Tonga-Kermadec island arc. *Earth Planet. Sci. Lett.* **179,** 581–593.

Turner S., Evans P., and Hawkesworth C. (2001) Ultrafast source-to-surface movement of melt at island arcs from ^{226}Ra-^{230}Th systematics. *Science* **292,** 1363–1366.

Wyllie P. J. (1979) Magmas and volatile components. *Am. Mineral.* **64,** 469–500.

Yogodzinski G. M., Lees J. M., Churikova T. G., Dorendorf F., Wöerner G., and Volynets O. N. (2001) Geochemical evidence for the melting of subducting oceanic lithosphere at plate edges. *Nature* **409,** 500–504.

Zack T., Rivers T., and Foley S. F. (2001) Cs-Rb-Ba systematics in phengite and amphibole: An assessment of fluid mobility at 2.0 GPa in eclogites from Trescolmen, Central Alps. *Contrib. Mineral. Petrol.* **140,** 651–669.